INFORMATION TO USERS

This manuscript has been reproduced from the microfilm master. UMI films the text directly from the original or copy submitted. Thus, some thesis and dissertation copies are in typewriter face, while others may be from any type of computer printer.

The quality of this reproduction is dependent upon the quality of the copy submitted. Broken or indistinct print, colored or poor quality illustrations and photographs, print bleedthrough, substandard margins, and improper alignment can adversely affect reproduction.

In the unlikely event that the author did not send UMI a complete manuscript and there are missing pages, these will be noted. Also, if unauthorized copyright material had to be removed, a note will indicate the deletion.

Oversize materials (e.g., maps, drawings, charts) are reproduced by sectioning the original, beginning at the upper left-hand corner and continuing from left to right in equal sections with small overlaps. Each original is also photographed in one exposure and is included in reduced form at the back of the book.

Photographs included in the original manuscript have been reproduced xerographically in this copy. Higher quality 6" x 9" black and white photographic prints are available for any photographs or illustrations appearing in this copy for an additional charge. Contact UMI directly to order.

UMI

A Bell & Howell Information Company
300 North Zeeb Road, Ann Arbor MI 48106-1346 USA
313/761-4700 800/521-0600

Université d'Ottawa · University of Ottawa

Time-Frequency Heart Rate Variability Spectral Analysis:

Effects of Unilateral Stellate Blockade

by

©KESAVA C. RAJAGOPALAN

A thesis submitted to the
School of Graduate Studies and Research
in partial fulfillment of the requirements
for the degree of

MASTER OF APPLIED SCIENCE
(Electrical Engineering)

UNIVERSITY OF OTTAWA
Ottawa, Ontario
1997

National Library of Canada
Acquisitions and Bibliographic Services
395 Wellington Street
Ottawa ON K1A 0N4
Canada

Bibliothèque nationale du Canada
Acquisitions et services bibliographiques
395, rue Wellington
Ottawa ON K1A 0N4
Canada

Your file Votre référence

Our file Notre référence

The author has granted a non-exclusive licence allowing the National Library of Canada to reproduce, loan, distribute or sell copies of his/her thesis by any means and in any form or format, making this thesis available to interested persons.

The author retains ownership of the copyright in his/her thesis. Neither the thesis nor substantial extracts from it may be printed or otherwise reproduced with the author's permission.

L'auteur a accordé une licence non exclusive permettant à la Bibliothèque nationale du Canada de reproduire, prêter, distribuer ou vendre des copies de sa thèse de quelque manière et sous quelque forme que ce soit pour mettre des exemplaires de cette thèse à la disposition des personnes intéressées.

L'auteur conserve la propriété du droit d'auteur qui protège sa thèse. Ni la thèse ni des extraits substantiels de celle-ci ne doivent être imprimés ou autrement reproduits sans son autorisation.

0-612-20945-8

Canada

Table of Contents

List of Figures

List of Tables

List of Symbols and Notation

< > - average value

ACH - acetylcholine

AMI - acute myocardial infarct

AP - arterial pressure

AR - autoregressive

BW - bandwidth

CNS - central nervous system

CV - cardiovascular

ECG - electrocardiograph

ED - exponential distribution

FFT - fast fourier transform

HF - high frequency

HR - heart rate

HRV - heart rate variability

IF - instantaneous frequency

LF - low frequency

NE - norephrinephrine

pts - points

RID - reduced interference distribution

RSA - respiratory sinus arrhythmia

SA - sino-atrial

SNR - signal to noise ratio

SPWD - smoothed pseudo-Wigner distribution

STFT - short-time fourier transform

TF - time-frequency

VLF - very high frequency

WD - Wigner distribution

Acknowledgments

I would like to express my gratitude to Drs N.U. Ahmed and T. Yeap for their encouragement and guidance in this work. In addition, I would like to thank Dr. S.T. Nugent from Dalhousie University for introducing me to the field of Heart Rate Variability. Finally, I would like to thank Dr. J.P. Finley from the Izaak Walton Killiam Hospital for obtaining the patient data that was used in this work.

Abstract

The Cohens class of time-frequency spectral analysis distributions are receiving significant attention in the signal processing field because of its appropriateness in analyzing time-varying signals. This work has investigated in detail the application of several Cohen class time frequency distributions to Heart Rate Variability Signals. The clinical application of these tools to these physiological signals has been limited. Using simulated nonstationary and stationary HRV signals, it has been shown that the time-frequency spectral estimators such as smoothed pseudo-Wigner and the exponential distribution offer better performance over the Short Time Fourier Transform in terms of resolution and ability to track the nonstationary behavior or instantaneous frequency if the parameters used in the distributions are carefully chosen. These time-frequency spectral analysis tools have been used as a means to quantify the autonomic tone for seven adults under the effects of right unilateral stellate blockade. The mean peak amplitudes under the predefined low frequency (LF) band (0.05-0.15 Hz) and high frequency band (0.15-0.45 Hz) were computed for pre and post blockade conditions in the supine and standing positions. These results have demonstrated the partial stellate blockade decreased the LF areas by 33% when standing and underlines the importance of efferents from the contralateral and higher cervical ganglia in the control of heart rate. In

conclusion, these time-frequency spectral analysis tools will provide the cardiologist with valuable diagnostic, cost effective and noninvasive information about the sympathetic and parasympathetic balance in patients to identify if they are at any medical risk.

Chapter 1

1. Introduction

Since the early eighties, investigators have recognized that spectral analysis of heart rate variability (HRV) signals could provide information on the cardiorespiratory control systems that modulate heart rate (HR) [Aks81][Pom85][Aks85]. This information provides valuable diagnostic information that can be readily and noninvasively derived from a single electrocardiograph (ECG) recording. Under normal conditions, the instantaneous HR and other hemodynamic parameters fluctuate on a beat to beat basis and exhibit a high degree of variability. HR is predominately modulated by the sympathetic and parasympathetic or vagal autonomic nervous system that innervates the sino-atrial (SA) node. A normal distribution of the RR intervals is indicative of autonomic balance. Decreased activity or no variability in the HRV spectrum provides an indication that abnormalities of these cardiorespiratory control systems or some degree of autonomic imbalance may exist placing the patient at some medical risk. When compared to time domain methods such as the mean, standard deviation, standard deviation of the RR intervals, it has been shown that power in predefined frequency bands provided the greatest differences in segregating patients with known cardiac dysfunctions [Mye86].

Therefore, HRV spectral analysis has found numerous clinical applications [Mye86] [Sau88] [Sin88] [Fin89] [Bia90] [Cra92][Hui93] [Big93].

Postural and selective autonomic blockade pharmacological studies have shown that three regions of activity could be identified in the HRV spectrum as shown in Figure 1.1 [Aks85][Pom85][Fin87] They are defined as follows: a) a very low frequency (VLF) band, 0-0.05 Hz b) a low frequency (LF) band, 0.05-0.15 Hz and c) a high frequency (HF) band, 0.15-0.45 Hz.

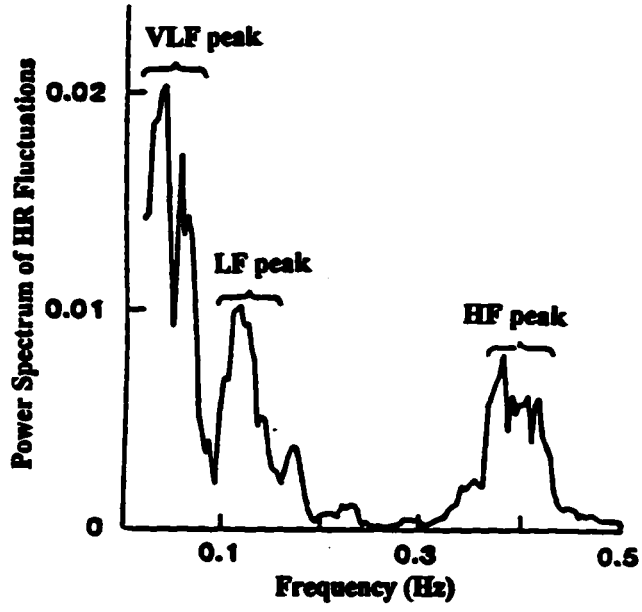

Figure 1.1 HRV spectrum of a normal individual

In these bands, distinct frequency peaks or oscillations can be found. The first is a VLF peak whose origin is believed to be from fluctuations in vasomotor tone. In addition, activation of the renin-angiotensin system has been found to damp these fluctuations [Aks81]. The exact mechanisms of this peak have not been

elucidated. The LF peak around 0.1 Hz arises from fluctuations in the baroreceptor reflex. This LF peak is both sympathetic and parasympathetic mediated. Orthostatic stress results in a dominant sympathetic spectral peak in this frequency band [Pom85][Nug86]. The third peak is seen at the respiration rate. Fluctuations in HR with a frequency equal to the breathing rate is known as respiratory sinus arrhythmia (RSA) and is mediated entirely by parasympathetic activity[Ang64] [Kat75]. Chapter 2 will review the autonomic control of HR, interpretation of the HRV signal, autonomic innervation, derivation of the HRV signal as well as to discuss the clinical uses of the HRV spectrum.

Conventional HRV spectral analysis techniques have been the Fast Fourier Transform (FFT) and autoregressive (AR) modeling[Kit92]. The traditional analysis approach is to divide the signal into data records that are assumed to be stationary and then to perform spectral averaging to obtain a decreased variance spectral estimate. These techniques are limited by the fact that they may not be suitable for the time varying nature of the HRV signal that originates from the interaction of these highly dynamic systems. The techniques require the assumption of stationarity and require the measurements to be taken under steady state conditions. In addition, these methods reveal frequencies that existed for the total duration of the signal, not frequencies that existed at a particular time which would allow for better clinical interpretation of the HRV spectrum. In order to circumvent these limitations, time-frequency (TF) spectral

analysis techniques provide a temporal-frequency history of the signal where a one dimensional signal of time s(t) is transformed into a two dimensional function of time and frequency $C(t,\omega)$. Attempts at tracking the instantaneous frequency (IF) changes in a signal include the popular Short Time Fourier Transform (STFT) or through the use of a running window AR estimator. Such methods are not optimal for the analysis of nonstationary signals. Recently, there has been considerable research directed towards a set of TF distributions that offer improved resolution and ability to track the IF. It has been shown that these bilinear or quadratic TF distributions can be derived from the following definition which is referred to as the Cohens class of TF distributions [Coh89]:

$$C(t,\omega)=\frac{1}{4\pi^2}\iiint s^*(u-\frac{\tau}{2})s(u+\frac{\tau}{2})\phi(\theta,\tau)e^{-j\theta t-j\tau\omega-j\theta u}dud\tau d\theta \quad (1.1)$$

$\phi(\theta,\tau)$ is a two dimensional function called the kernel. Various kernels have been derived with each having it own merits. Caution must be exercised with the use of these techniques with multicomponent signals as the interpretation of the spectrum can be obscured with crossterms. For example, the Wigner distribution uses a kernel of $\phi(\theta,\tau)=1$ and is plagued by artifacts or cross terms[Hla92]. The practical implementation of the Wigner distribution requires some degree of smoothing to suppress cross terms. Such an implementation is referred to as the smoothed pseudo-Wigner (SPWD) distribution. One such distribution that

attempts to improve on the Wigner distribution while at the same time minimizing cross terms is the exponential distribution (ED)[Cho89]. The ED is a member of the Cohens class are referred to as a reduced interference distribution (RID). Chapter 3 will review these distributions and their properties that make them unique.

Unfortunately, no single TF distribution can be determined as the best method as this depends on the signal being studied. The Cohens class of TF distributions have only recently received attention as being a valuable tool in analyzing physiological signals. It is critical to understand the effects of the parameters that are used in these distributions so that they are properly implemented so that the clinical results can be correctly interpreted. Chapter 4 will investigate the performance of the SPWD and the ED using simulated nonstationary and stationary HRV signals. Their performance will be compared against the STFT. Limited studies have adequately addressed the impact of the selection of the parameters on the performance of the distribution. This comparative study will address issues such as the resolution, crossterms behavior, ability to track the IF, statistical properties and the signal to noise ratio (SNR) performance. To the authors knowledge, the SPWD and ED has not been applied as a clinical tool in the analysis of the HRV signal. Chapter 5 will apply these TF distributions to patients who have undergone unilateral right stellate blockade to demonstrate their potential clinical viability.

Chapter 2

2 Heart Rate Variability

2.1 Autonomic Control of Heart Rate

HR is predominately modulated by the autonomic efferents that act on the SA node. A brief review of the cardiac sympathetic and parasympathetic nervous system will be presented. The mechanisms underlying HRV consist of the net sympathetic and parasympathetic influences on the SA node which is located at the junction of the superior vena cava and right atrium. In cardiac tissue, the SA node dominates cardiac rhythm because it has the highest intrinsic depolarization rate compared to all other tissues in the myocardium. This rhythmic self excitation of the SA node is due to the fact that the SA nodal fibers are very permeable to Na^+ ions. Figure 2.1 shows the rhythmic discharge of the SA node and ventricular fibers. The increased permeability of Na^+ to the SA node causes the resting potential to rise at a faster rate until it reaches the depolarization threshold. The repetition frequency or alternatively the length of the cardiac cycle is primarily reflected in the resting potential duration as all the other phases of this action potential remain generally invariant. The duration of this phase is determined by the rate of slow depolarization required to reach the depolarization threshold. In the absence of external influences this cycle repeats

itself regularly however under the effects of sympathetic and parasympathetic innervation, neurotransmitter release at the SA node can affect the slope of the phase, hence augmenting or inhibiting HR.

Sympathetic activity augments HR by modulating the SA node. Post ganglionic cells that innervate the heart secrete neurotransmitters that stimulate β-adrenergic receptors. There is a release of norephrinephrine (NE) which increases the membrane permeability to Na^+ ions. The result of this is to increase the SA node resting potential slope resulting in closer depolarizations.

The overall effect of parasympathetic activity is to decrease chronotropism. Stimulation of the parasympathetic nerves causes the release of acetylcholine (ACH) at the vagal endings. This increases the permeability of cardiac fibers to K^+ which results in a decreased resting potential slope thereby slowing down the depolarization rate resulting in a decreased HR.

2.1 Mechanisms underlying the HRV Spectrum Components

2.1.1 Baroreflex Peak

The central nervous system (CNS) plays an important part in HRV as it obtains information from various afferents within the CV system and modulates the autonomic nerves and endocrine cells in order to maintain an adequate arterial pressure (AP) via modulation of the HR and contractility (i.e. AP=HR*cardiac

output). In addition, these afferents can enter higher centers such as the hypothalamus and cortex. Of interest here are the afferent fibers that originate from arterial and cardiopulmonary mechanoreceptors that terminate in the solitary tract nucleus as shown in Figure 2.2

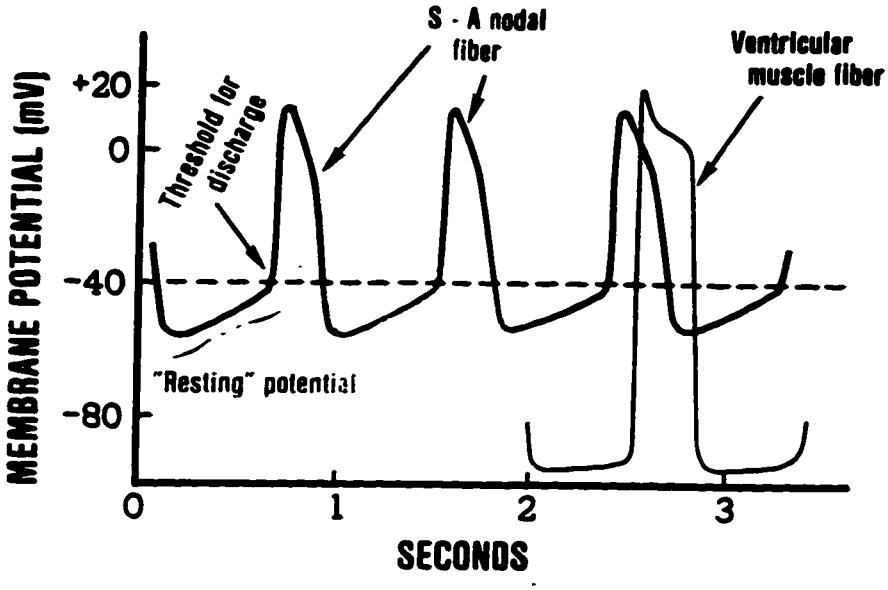

Figure 2.1 Rhythmic discharge of the SA node and comparison with that of a ventricular muscle fiber

At a more detailed level, there exists receptors in the walls of the internal carotids and the aortic arch or baroreceptors as shown in Figure 2.2 When the receptors are stretched by an increase in AP these receptors send signals via branches of the glossopharyngeal (carotid impulses) and vagal (aortic impulses) cranial nerves to the CNS for integration. These afferent signals enter the brainstem where they synapse with cells of the solitary tract nucleus. There are relays from here to the dorsal vagal nucleus and to the paramedian reticular nuclei of the vasomotor

center. Under the effects of increased AP or orthostatic stress, the vagal efferents will increase its inhibitory parasympathetic signals to the SA node decreasing HR. However, it does not end here, the sympathetic signal will decease normal firing or activity via the spinal cord from the vasomotor center to the peripheral effectors via the spinal cord. In addition, in another parallel route from the cardioinhibitory center, 5-hydroxytryptamine is released that decreases the release of NE. The interplay of the pressor and depressor provides the major control of the vasomotor tone by increasing the number of impulses that leave the spinal cord through the final common pathway, the preganglionic adrenergic neuron that releases ACH at the nerve endings in the sympathetic ganglia. This leads to activation of the postganglionic neurons which control the response of the heart by the amount of NE that is liberated. As mentioned earlier, NE acts on β-adrenergic receptors which results in an increased HR, conduction velocity and contractility.

The 0.1 Hz oscillation which is observed the HRV spectrum arises from fluctuations in the baroreceptor reflex. This oscillation is called the Mayer wave and is thought to arise from latencies in the baroreflex arc. The characteristics have been studied by numerous individuals and these studies along with computer modeling have confirmed that there is evidence of a pure time delay of approximately 2-4.5 seconds[Kit85]. This LF peak is both parasympathetic and sympathetic mediated as described earlier. Orthostatic stress studies result in a dominant sympathetic spectral peak in this frequency band [Pom85][Nug86]

[Vyb89]. Longer delays have been observed in children [Gid85] and in diabetic neuropathy patients [Van83]. These have been attributed to an immature autonomic system and degeneration of the sympathetic fibers resulting in slower conduction velocity respectively.

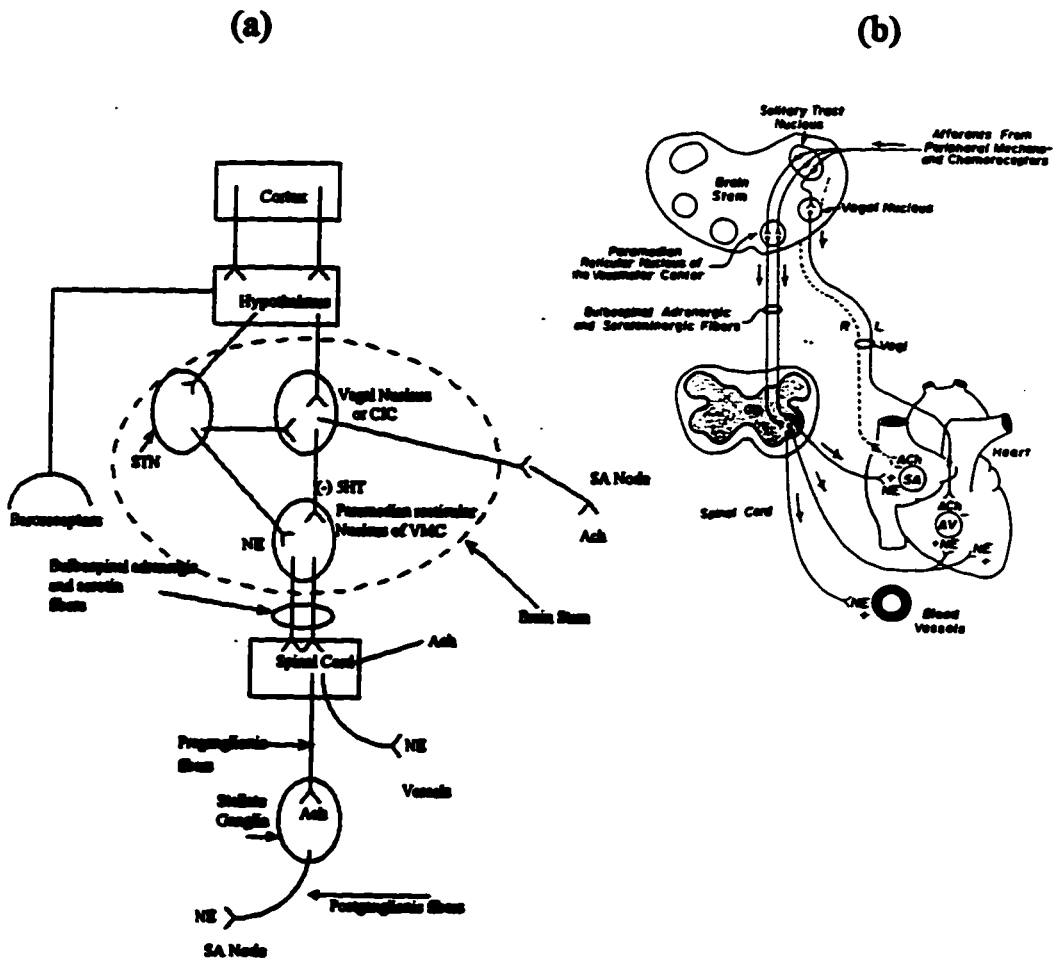

Figure 2.2 a) Autonomic control of circulation Origin and b) distribution of cholinergic and adrenergic nerves to the CV system

2.1.2 Respiration Peak

In respiration, pulmonary receptors inhibit the cardioinhibitory centers where vagal afferents increase their activity as the airway widens and the lung volume augments during inspiration as shown in Figure 2.3. The increased afferent traffic also inhibits the respiratory center causing inspiration to cease and expiration to begin. This is called the Hering-Traube inhibitory respiratory reflex that provides the optimal rate and depth of breathing with the least minimal energy expenditure. Lung inflation causes increased HR.

Fluctuations in HR with a frequency equal to the breathing rate is known as respiratory sinus arrhythmia (RSA). RSA has been suggested to result from: a) a lung inflation reflex which causes cardiac acceleration b) interaction between the respiratory centers and the autonomic control of HR c) increased filling of the right atrium during inspiration as a cause of cardiac acceleration and d) central modulation of the baroreflex. It is unknown as to whether RSA is due to a direct effect of respiration on the reflex or as an indirect effect mediated by thoracic volume receptors[Sau89]. Other studies suggest that RSA can be considered as the interaction of two nonlinear systems, respiration and the baroreflex[Kit85]. In adults, this phenomena can be considered in terms of entrainment of the 0.1 Hz baroreflex component by the dominant respiratory component. In neonates this interaction is not as apparent as the breathing rate is

on the order of 50 breaths/minute. At this frequency of 0.8 Hz, the respiratory frequency is sufficiently removed from the 0.1 Hz component and entrainment probably does not occur.

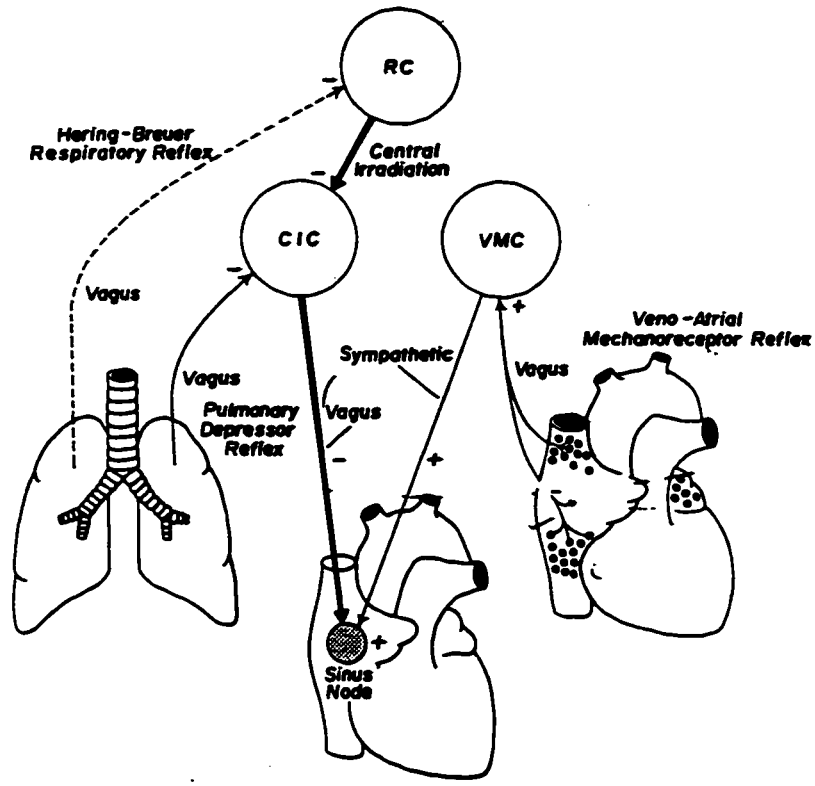

Figure 2.3 Mechanisms involved in respiratory sinus arrhythmia

2.3 Sympathetic Innervation

The distribution of sympathetic nerves to the heart is very complex. As mentioned earlier the overall effect of these sympathetic postganglionic neurons is to augment HR and cardiac inotropism. Most of the current literature describing

the distribution of sympathetic efferents to the heart has been inconsistent. Janes et al describe in detail the origin and distribution of the left and right cardiopulmonary nerves arising from the ganglia chain in cadavers[Jan86]. Sympathetic nerves that innervate the heart consist of axons that originate from the spinal cord between segments C8 (cervical ganglia) to T2 (thoracic ganglia) as shown in Figure 2.5. Preganglionic nerves that originate from the stellate ganglia and caudal halves of the cervical sympathetic trunk synapse with postganglionic nerves. There is evidence to suggest that no sympathetic nerves were found to originate from the superior cervical ganglion and thoracic sympathetic trunks. It has been observed that all sympathetic cardiopulmonary nerves were found to originate from the stellate ganglia and caudal halves of the middle cervical ganglia and thoracic sympathetic trunks inferior to the stellate ganglia.

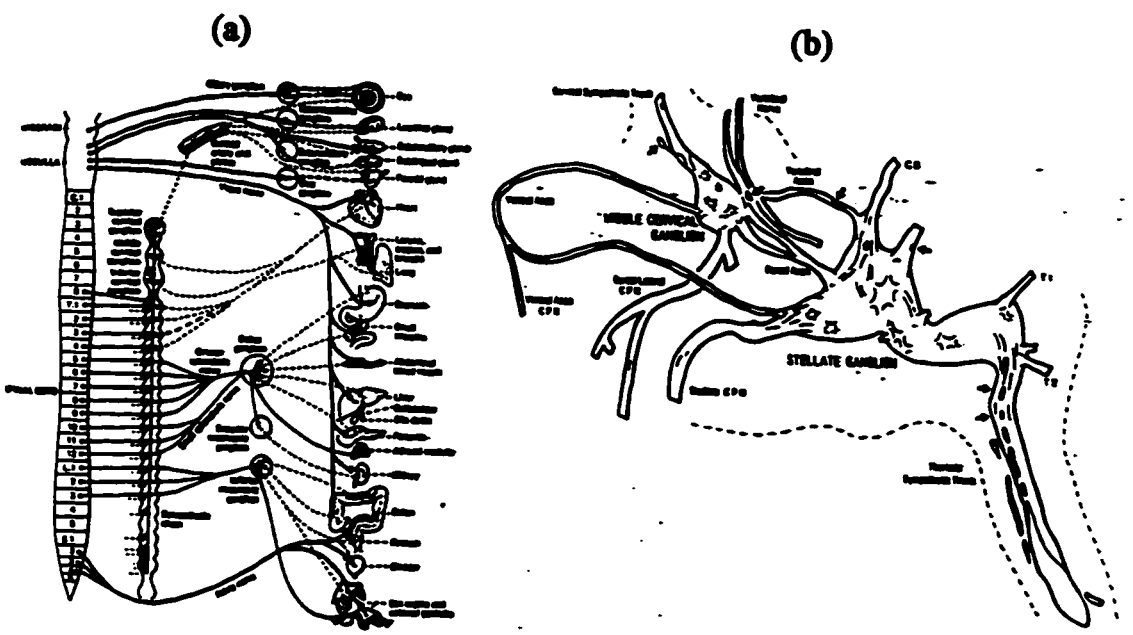

Figure 2.4 a) Autonomic efferent pathways and b) Sympathetic ganglia

The right stellate cardiopulmonary nerves usually compromise 3 major nerves that arise from the region of the right stellate and middle cervical ganglia. These nerves project in the SA nodal area where it joins with other cardiopulmonary nerves. The left stellate, left dorsal medial and left dorsal lateral cardiopulmonary nerve eventually connect with the nerves from the right side. In addition, the right and left cardiopulmonary nerves interconnect in the plexus regions of the mediastinum. From this plexus many small nerves extensively innervate the adjacent atria, aorta, pulmonary artery pulmonary veins and trachea.

This anatomical review shows that the distribution of sympathetic nerves to the heart is very complex with the SA nodal area being innervated by the right side cardiopulmonary nerves and contralateral innervation from the left side and nerves arising from the plexus region of the mediastinum. This differs from traditional views where it was believed that right side cardiopulmonary nerves predominately innervate the SA nodal area.

In this work an application involving the blockade of the right stellate blockade will be studied. Typically, pharmacological blockade or surgical deinnervation of the sympathetic stellate chain is used for the management of angina, cardiac rhythm disturbances, ischemic pain, tachycardia, removal of vasoconstrictor tone and sympathetic imbalance [Sch87].

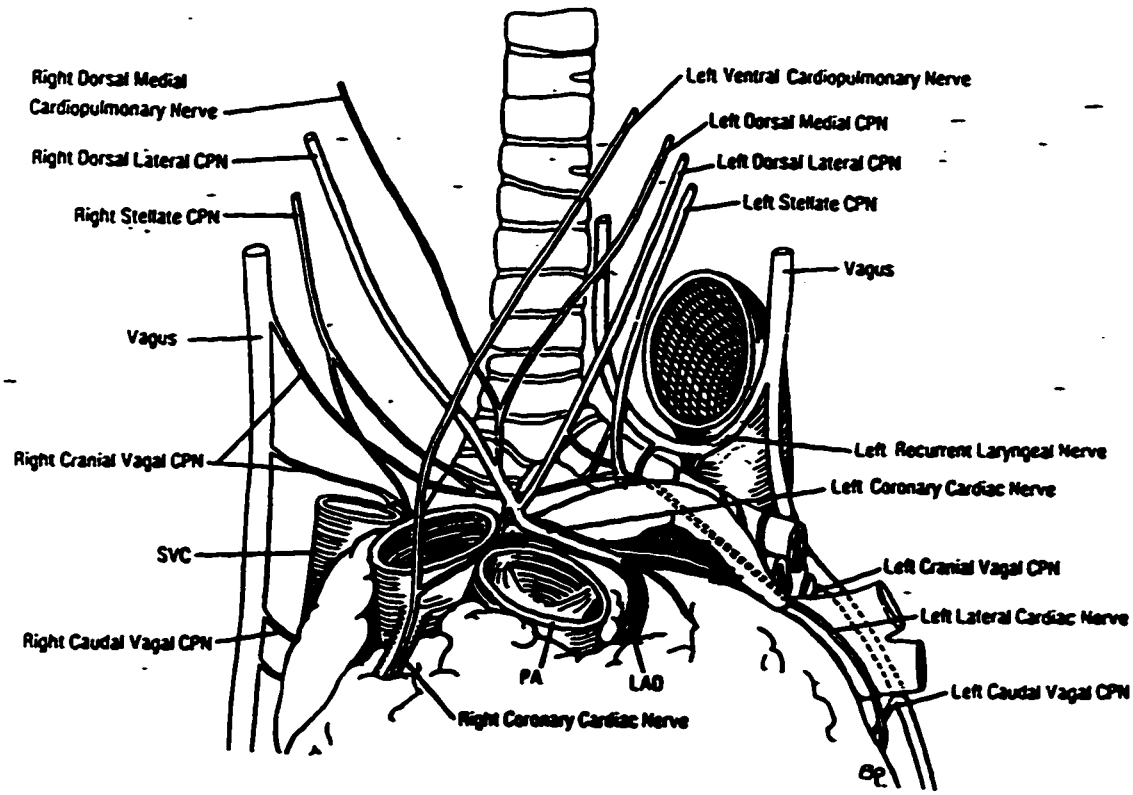

Figure 2.5 Distribution of the sympathetic and parasympathetic efferents to the heart

2.4 Parasympathetic Innervation

Parasympathetic nerves were found to arise from the recurrent laryngeal nerves and the thoracic vagi as seen in Figure 2.5. Left and right vagal nerves interconnect with sympathetic cardiopulmonary nerves anterior and posterior to the main pulmonary artery and from the plexus region which subsequently innervates the atria, aorta pulmonary atria, pulmonary veins and trachea. The right vagus tends to distribute mainly to the SA node whereas the left vagus mainly to the AV node.

2.5 Derivation of the Heart Rate Variability Signal

This section discusses methods used to derive a HRV signal from the ECG. The first step is to reduce the ECG to a event process where the events are the R-wave occurrence times of the QRS complexes as shown in Figure 2.6. It has been suggested that this signal must be sampled at a rate of > 300 Hz so that there are no appreciable errors in the HRV spectrum.[Rom87] Having identified the R-waves of the ECG, the data is defined at irregular intervals. Spectral estimation algorithms assume regularly sampled intervals, therefore it is necessary to convert this point process into a regularly spaced sampled signal. There are four principal techniques that have been defined to derive a HRV signal from cardiac event series which are the interval tachogram, interpolated, inverse intervals and the low pass filtered event series [Rom77]. In the comparison of these methods only minor differences in the spectrum were observed when using a simulated HRV signal [deB85]. In this work the method of inverse intervals will be used. This method generates the reciprocals of successive RR intervals as shown in Figure 2.6 and is given by the expression

$$HRV(i) = 1/(t(i) - t(i-1)) \quad (2.1)$$

where t(i) is defined as the R-wave occurrence.

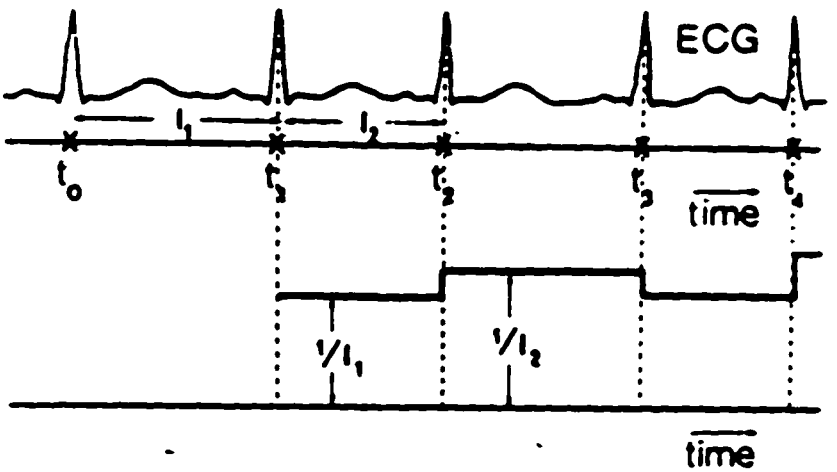

Figure 2.6 Derivation of the HRV signal using the method of inverse intervals

2.6 Clinical Implications of Heart Rate Variability Spectral Analysis

As mentioned earlier, several investigators have identified three regions of activity in the spontaneous HRV spectrum of healthy adults, a low frequency region around 0.05 Hz due to thermoregulation, a component around 0.1 Hz arising from baroreceptor activity and a component at the respiratory frequency. The role of HRV spectral analysis has found numerous clinical applications. Decreased power on these frequency bands may signify some degree of autonomic imbalance. For example, condition of sympathetic hyperactivity, lack of protective vagal tone or total absence of autonomic tone maybe indicative of serious clinical problems. A high degree of HRV is noted in a normal CV system where decreased power in the HRV spectrum can be seen with patients with

atrial septal defect[Fin89] diabetic neuropathy[Bia90],severe coronary artery disease[Hui93], congestive heart failure [Sau88], acute myocardial infarct(AMI) [Kle87] [Lom87] [Big88] [Big93a] [Big93b] [Cra92]and sudden cardiac death [Mye86][Sin88]. The underlying rationale of these studies is that abnormal autonomic control of CV function such as decreased parasympathetic activity or RSA activity may predispose the heart to ventricular fibrillation. Transient ischemic episodes usually associated with signs of sympathetic hyperactivity could be triggered. Reduced power in the HRV spectrum carries a poor prognosis in post AMI patients[Mal90].

HRV spectral analysis has been used as an unique method in establishing the state of reinnervation in post transplant patients. Studies have demonstrated that functional reinnervation of the human heart allograft can occur [Fal88]. In addition, it has been suggested that the spectrum of myocardial rejection patients consisted of broad based oscillations where the total spectrum was quite generous[San86].

These studies have shown that HRV spectral analysis is a valuable noninvasive tool in establishing the diagnosis, prognosis and management of these patients.

Chapter 3

3. Time-Frequency Spectral Analysis

3.1 Introduction

In the last few years considerable research has been focused towards TF spectral analysis in the attempt to obtain suitable distributions that allow simultaneous representation of a signal in the time and frequency domain. Its use is particularly valuable in the analysis of nonstationary or time-varying signals. TF spectral analysis maps an one dimensional signal of time $s(t)$ into a two dimensional function of time and frequency $C(t, \omega)$. The variation of the spectral components can be readily determined with respect to time. For example, in performing HRV spectral analysis, the underlying pathophysiological condition and/or interactions of the cardiorespiratory system can make the signal highly nonstationary. The general approach in handling these signals for spectral estimations algorithms is to window the signal. Within this short duration window the signal can be assumed to be wide-sense stationary. A wide-stationary process, $s(t)$ is defined as one for which its mean is constant for all time and the autocorrelation function is independent of time and is a function of the lag k only.

$$R(k) = E\{s(n+k)s^*(n)\} \quad (3.1)$$

One such popular TF representation is the STFT or the spectrogram (magnitude squared of the STFT). It has found numerous applications as a result of its ease of implementation. Recently, there has been considerable interest in more sophisticated quadratic or bilinear distributions that are capable of higher resolution spectral estimates and which are able to track the IF of a time-varying signal with better accuracy. It can be shown that the IF which will be defined later in the chapter, can be exactly derived from these distributions. These methods may offer significant advantages in the analysis of nonstationary physiological signals such as the HRV signal. These bilinear or quadratic distributions belong to a group of distributions referred to as the Cohen class of distributions. Popular TF distributions from this class include the WD and the RID such as the ED. In this section, the properties of these TF distributions are reviewed and compared to the STFT to illustrate their advantages.

3.2 Cohens Class of Time-Frequency Distributions

Many TF representations can be written in a unified definition which was proposed by Cohen[Coh89]:

$$C(t,\omega)=\frac{1}{4\pi^2}\iiint s^*(u-\frac{\tau}{2})s(u+\frac{\tau}{2})\phi(\theta,\tau)e^{-j\theta t-j\tau\omega-j\theta u}dud\tau d\theta \quad (3.2)$$

$s(t)$ is the analytic signal and $\phi(\theta,\tau)$ is a two dimensional function called the kernel. This term was introduced by Classen and Mecklenbrauker[Cla80a]. The kernel allows one to determine the distribution and its properties.

3.2.1 Characteristic Function

The characteristic function has been defined as one useful way to study TF distributions and is a valuable tool in kernel design. It is introduced in this chapter to demonstrate the alternate and reduced forms that the distributions can be viewed and compared. It is defined as the double Fourier transform of the distribution as shown below[Coh89]

$$M(\theta,\tau)=\left\langle e^{j\theta+j\tau\omega}\right\rangle=\iint C(t,\omega)e^{j\theta+j\tau\omega}dtd\omega \quad (3.3)$$

It allows one to readily compute the IF and second moments by differentiation rather than integration. A TF distribution can be described in terms of its characteristic equation as shown below:

$$C(t,\omega)=\frac{1}{4\pi^2}\iint M(\theta,\tau)e^{-j\theta-j\tau\omega}d\theta\,d\tau \qquad (3.4)$$

where

$$M(\theta,\tau)=\phi(\theta,\tau)\int s^*(u-\frac{\tau}{2})s(u+\frac{\tau}{2})e^{j\theta u}du=\phi(\theta,\tau)A(\theta,\tau) \quad (3.5)$$

$A(\theta,\tau)$ is defined as the symmetrical ambiguity function. The characteristic function has also been referred to as the generalized ambiguity function[Coh85]. If it were possible to find the characteristic function we could obtain the distribution from the equation above. Alternatively, if the distribution is given one can determine the kernel by

$$\phi(\theta,\tau)=\frac{M(\theta,\tau)}{A(\theta,\tau)}=\frac{\iint C(t,\omega)e^{j\theta+j\omega}dtd\omega}{\int s^*(u-\frac{\tau}{2})s(u+\frac{\tau}{2})e^{j\theta u}du} \quad (3.6)$$

3.2.2 Distribution and Kernel Properties

There are several advantages in characterizing the TF distribution by the kernel function which include the following 1) by constraining the kernel one can obtain and study the distributions 2) by examining the kernel the properties of the distribution can be determined and 3) given a kernel the distribution can be easily generated[Jeo92]. The degree of resolution and crossterm tradeoff depends on the kernel $\phi(\theta,\tau)$ that is used. Table 3.1 outlines some of the kernels that will be examined in this work.

Table 3.1 Kernels for various distributions

Distribution	Kernel $\phi(\theta,\tau)$
Spectrogram	$A_w(\theta,\tau)$ (ambiguity function of a window function)
Wigner	1
Exponential	$e^{-\theta^2\tau^2/\sigma}$

There is no consensus on the exact properties and the number of required properties that a distribution must satisfy as each author outlines his own [Hla92][Boa90][Coh89][Wil95]. A summary of the desirable properties of the distribution and the kernels are noted below.

Positivity: A distribution should be positive for all values of time and frequency where $C(t,\omega) \geq 0$. The Wigner and most TF distributions are rarely positive. The significance of the negative parts of the spectrum are unclear however it is believed that the positive part carries the physical information[Coh89]. In addition, the cross terms which have no physical significance can oscillate and go negative and this is shown in section 3.2.3.

Instantaneous Energy and Spectrum: By integrating the TF distribution with respect to time and frequency, we must be able to obtain the instantaneous power $|s(t)|^2$ and the energy density $|S(\omega)|^2$ respectively. For example, in order to obtain the instantaneous power, by integrating equation 3.2 with respect to frequency it is required that $\phi(\theta,0) = 1$ be satisfied so that the time marginal is satisfied. Similarly, $\phi(0,\tau) = 1$ for the frequency marginal to be satisfied.

Total Energy: In order for the energy to be preserved i.e. $\int_{-\infty}^{\infty}\int_{-\infty}^{\infty} C(t,\omega)dtd\omega = 1$ we must have $\phi(0,0) = 1$

Reality: We know that $M(\theta,\tau)=\phi(\theta,\tau)A(\theta,\tau)$ and it can readily be shown that $A(\theta,\tau)=A^*(-\theta,-\tau)$ for the ambiguity function therefore for the distribution to be real the characteristic function must satisfy $M(\theta,\tau)=M^*(-\theta,-\tau)$. The necessary and sufficient condition for the distribution to be real requires the kernel to satisfy the following condition: $\phi(\theta,\tau)=\phi^*(-\theta,-\tau)$.

Time and Frequency Shifts: If the signal $g(t)=e^{j\omega t}s(t-t_0)$ is introduced such that a time and frequency shift is introduced. Then the distribution is expected to be shifted by the same amount i.e. $C_g(t,\omega)=C(t-t_0,\omega-\omega_0)$. It is required that the kernel is not a function of time and frequency.

Scaling Invariance: If we scale $g(t)=\sqrt{a}s(a/t)$ then the spectrum must be inversely scaled such that $C_g(t,\omega)=C(at,\omega/a)$. In order for this to be true $\phi(a\theta,\tau/a)=\phi(\theta,\tau)$. For scale invariance $\phi(\theta,\tau)=\phi(\theta\tau)$ must be a product kernel.

Weak finite time and frequency Support: For a signal that has finite duration we require that the distribution be zero before and after the signal starts and ends respectively. This condition requires $\int\phi(\theta,\tau)e^{-j\theta t}dt=0$ for $|\tau|\le 2|t|$. A similar definition holds for the frequency.

Strong finite support: This means that the distribution is zero whenever the signal or spectrum is zero. The condition for this requires $\int\phi(\theta,\tau)e^{-j\theta t}dt=0$ for $|\tau|\ne 2|t|$. A similar definition holds for the frequency.

IF: The IF is an important quantity in TF analysis and is defined as follows

$$\omega_i(t) = \frac{\int \omega C(t,\omega) d\omega}{\int C(t,\omega) d\omega} = \varphi'(t) \quad (3.7)$$

The requirement for this to be equal to the derivative of the phase requires that $\frac{\partial \phi(\theta,\tau)}{\partial \theta}|_{\tau=0} = 0$ and the time marginal must be satisfied $\phi(\theta,0) = 1$.

Group Delay: The group delay is defined as follows:

$$t_g(\omega) = \frac{\int tC(t,\omega) dt}{\int C(t,\omega) dt} = -\psi'(t) \quad (3.8)$$

The requirement for the group delay to be equal to the derivative of the spectral phase requires that $\frac{\partial \phi(\theta,\tau)}{\partial \theta}|_{\theta=0} = 0$ and the time marginal must be satisfied $\phi(0,\tau) = 1$. Table 3.2 provides a comparison of the different distributions.

Table 3.2 Comparison of the different distributions

Kernel Feature	Spectrogram	Wigner	Exponential
positivity	+	-	-
time and frequency marginals	-	+	+
reality	+	+	+
time and frequency shifts	+	+	+
scaling invariance	+	+	+
time and frequency support	-	+	-
IF and group delay	-	+	+

(+) property satisfied (-) property not satisfied

3.2.3 Cross Terms

The practical use of the quadratic or bilinear TF distributions are limited by the presence of cross terms. Cross terms are extraneous terms that lie between two autocomponents. For multicomponent signals the inherent bilinear structure of Cohens class distributions causes interfering crossterms which do not permit a straight forward interpretation of the energy distribution and are these crossterms could become troublesome when one wishes to use TF features for pattern recognition and classification applications. The amount and shape of the interference can be controlled by kernel which may be able to these suppress cross terms. In order to illustrate this important point consider the following example. The WD is defined in equation:

$$WD(t,\omega)=\frac{1}{2\pi}\int s^{*}(t-\frac{\tau}{2})s\ (t+\frac{\tau}{2})e^{-j\omega}d\tau \quad (3.9)$$

Consider the following multicomponent signal which consists of two terms $s(t)=s_1(t)+s_2(t)$ where $s_1(t)=A_1e^{j\omega_1 t}$ and $s_2(t)=A_2e^{j\omega_2 t}$. Substituting this into the definition we have

$$WD(t,\omega)=WD_{11}(t,\omega)+WD_{22}(t,\omega)+WD_{12}(t,\omega)+WD_{21}(t,\omega) \quad (3.10)$$

It can be readily shown that that $WD_{12}=WD_{21}$. In addition. $WD_{12}(t,\omega),WD_{21}(t,\omega)$ are real so that

$$WD(t,\omega)=\ WD_{11}(t,\omega)+\ WD_{22}(t,\omega)+\ 2\,\mathrm{Re}\{WD_{12}(t,\omega)\} \quad (3.11)$$

Therefore the WD of s(t) is

$$WD(t,\omega) = A_1^2\delta(\omega-\omega_1) + A_2^2\delta(\omega-\omega_1) + 2A_1A_2\delta(\omega-\frac{1}{2}(\omega_1+\omega_2))\cos(\omega_2-\omega_1)t \quad (3.12)$$

There are two autoterms at ω_1 and ω_2 In addition we have an oscillating cross term at $\frac{1}{2}(\omega_1+\omega_2)$. In general, Hlawatsch et al has shown that the number of cross terms is N(N-1)/2 where N is the number of signals[Hla92]. Several techniques exist to minimize the effects of cross terms. These include a) the use of the analytic signal that is described in section 3.4 b) use of a time smoothing window and c) an effective kernel should be able to diminish the effects of interfering crossterms. The tradeoff when using these techniques is that there maybe a compromise in resolution.

3.3 Time-Frequency Distributions

3.3.1 Short-Time Fourier Transform

The STFT assumes that for a short-time basis, the signal s(t) can be considered stationary or time invariant. The main advantage of this method is that it is computationally efficient and easily implemented. In the STFT, time localization of the frequency components can be obtained by suitable prewindowing with the use of a real symmetric window such that

$s_t(\tau) = s(\tau)h(\tau - t)$. The local spectrum is obtained around the analysis time t. The squared magnitude of the STFT or spectrogram is given in equation 3.13

$$|STFT(t,\omega)|^2 = \left|\frac{1}{\sqrt{2\pi}}\int s(\tau)h(\tau - t)e^{-j\omega\tau}d\tau\right|^2 \quad (3.13)$$

The spectrogram can be considered in terms of the Cohens class of TF distributions. The characteristic function of the spectrogram can be derived to show that it is the ambiguity function of the signal times that of the window.

$$M_{SPEC}(\theta,\tau) = A\ (\theta,\tau)A_w(-\theta,\tau) \qquad (3.14)$$

Therefore, the

$$\phi_{Spec}(\theta,\tau) = \frac{M_{SPEC}(\theta,\tau)}{A(\theta,\tau)} = \mathrm{A}_w(-\theta,\tau) \quad (3.15)$$

The main disadvantage of this method is that there is a tradeoff between temporal and frequency resolution. This is due to the uncertainty principle that states that the time bandwidth product for the STFT is equal to a constant.

$$TB \geq \frac{1}{2} \quad (3.16)$$

where T and B are defined as the time and frequency spread respectively. They are defined as follows: $T^2 = \int (t - < t >)^2 |s(t)|^2 dt$ and $B^2 = \int (\omega - < \omega >)^2 |S(\omega)|^2 d\omega$. The uncertainty principle prohibits the existence of windows with small durations and small BW. To increase the frequency resolution one must use a longer observation window, then the assumption of stationarity is violated. Good time resolution of

the STFT requires a short time window, then the BW becomes infinite. The spectrogram can also be viewed as the 2D convolution of the WD of the signal and the window[Cla80c]

$$|STFT(t,\omega)|^2 = \frac{1}{2\pi} WD_s(t,\omega) * WD_w(-t,\omega) \quad (3.17)$$

Of particular interest is the IF of the STFT which is defined as the conditional average frequency at time t. The expression depends on both the signal and the window and it has been shown that as the window approaches the δ function, we approach the IF. However the tradeoff is that by narrowing this window we broaden the standard deviation or spread about the IF i.e. $\sigma_{w/t} \to \infty$. The optimal STFT requires a priori knowledge of the IF. For pure linearly modulated signals, it has been shown that the optimal window length is related to the IF frequency by [Boa90]

$$\Delta = \left| \frac{df_i(t)}{dt} \right|^{-1/2} \quad (3.18)$$

3.3.2 Wigner Distribution

One of the original TF distributions is the Wigner-Ville distribution which is defined as follows.

$$WD(t,\omega) = \frac{1}{2\pi} \int s^*(t - \frac{\tau}{2}) s(t + \frac{\tau}{2}) e^{-j\omega\tau} d\tau \quad (3.19)$$

The WD is a nonlocal function where equal weight is given for all times. The characteristic function of the WD is defined as:

$$M(\theta,\tau)=\iint e^{j\theta t+j\omega\tau}WD(t,\omega)dtd\omega=\int s^{*}(t-\frac{\tau}{2})s(t+\frac{\tau}{2})e^{j\theta t}dt=A(\theta,\tau) \quad (3.20)$$

where s(t) is either a real or complex valued signal. Therefore the kernel is one and is shown in Figure 3.1 The WD always satisfies the marginals and because of this the total energy is equal to 1. The time and frequency shifts property is satisfied as well as definitions for the mean time, mean frequency, bandwidth. One can obtain exact expressions for the IF and the group delay directly from the WD definition for monocomponent signals [Cla80b] The IF is derived exactly derived as $\phi'(t)$.

As a result of the nonlocal definition of the WD, cross terms exist for multicomponent signals as described earlier. Practical implementation of the WD is accomplished by incorporating some degree of time smoothing to remove these oscillating terms. By low pass filtering the WD at the expense of autocomponent broadening we can minimize the effects of cross terms. Such an implementation is referred to as the SPWD that is defined below

$$SPWD(t,\omega)=\frac{1}{2\pi}\int|h(\tau/2)|^{2}\{\int g(t-u)s^{*}(u-\frac{\tau}{2})s(u+\frac{\tau}{2})du\}e^{-j\omega\tau}d\tau \quad (3.21)$$

where g(t) is a time smoothing window and h(τ) is a frequency smoothing window. In addition the PSWD can be viewed as the convolution of a filter $F(t,\omega)$ and the WD of the signal $WD_{s}(t,\omega)$.

$$SPWD(t,\omega) = \frac{1}{2\pi} WD_s(t,\omega) * F(t,\omega) \quad (3.22)$$

Unlike the STFT, one is not constrained by the uncertainty principle where independent time and frequency resolution can exist. By windowing the lag we attempt to emphasize the properties of the signal at time t and at the same time some of the desirable properties of the WD are lost. The marginals and the IF do not hold anymore. In the use of the SPWD there is a tradeoff between good interference attenuation and good TF resolution. A broad WD smoothing domain yields good interference attenuation but poor resolution whereas a narrow smoothing function yields poor interference attenuation but good TF resolution.

3.3.3 Exponential Distribution

Another Cohen class TF distribution has been developed by Choi et al and is referred as the Choi-Williams or exponential distribution (ED) [Cho89]. It belongs to a class of reduced interference distributions (RID) that has showed promising results for multicomponent signals by significantly attenuating cross terms artifacts while at the same time preserving desirable properties of the WD. It is defined as follows:

$$ED(t,\omega) = \sqrt{\frac{\sigma}{4\pi^3}} \iint \frac{1}{\tau} e^{\left(-\sigma\frac{(u-t)^2}{4\tau^2} - j\tau\omega\right)} s^*(u - \frac{\tau}{2}) s(u + \frac{\tau}{2}) du d\tau \quad (3.23)$$

An exponential kernel was found to be a good choice in order to minimize the effects of the cross terms and still satisfy the desirable properties of a distribution such as reality, frequency shift and marginals. The exponential kernel is defined as follows and is shown in Figure 3.1.

$$\phi_{ED}(\theta,\tau) = e^{-\theta^2\tau^2/\sigma} \quad (3.24)$$

The motivation of the design of such RID has been described by attempting to minimizing the cross terms under the following constraint $\phi(\theta,\tau) << 1$ for $\theta\tau >> 0$[Jeo92]. If we examine this constraint with respect to the WD that has the value of one in the $\theta\tau$ plane, this does not satisfy the cross minimization property. For the spectrogram, if a Hamming window is used one notes that the kernel is peaked at the origin and tapers off. This accounts for the good cross term minimization by the spectrogram however as mentioned before it does not satisfy the marginals and is constrained by the uncertainty principle. The ED is peaked at the center and the parameter σ is adjusted to control the fall off and can be adjusted to obtain the best compromise in terms of resolution and cross terms suppression. As $\sigma \rightarrow \infty$, the ED approaches the WD because the kernel becomes flat and there will be no cross term suppression. The exponential RID can be viewed as using a smoothed version of the time-dependent autocorrelation function. The exponential kernel is used to emphasize temporally close instantaneous autocorrelation function values but incorporates greater averaging as

the lag variable τ increases. The exponential product kernel and therefore the distribution preserves the signal energy marginals. i.e. $\phi(0,\tau)=\phi(\theta,0)=1$. The IF condition is satisfied as $\sigma \rightarrow \infty$.

3.4 The Analytic Signal

The Cohen class of TF distributions requires the extensive use of the analytic signal, $s(t)$ which is defined below as

$$s(t) = x(t) + H\{x(t)\} \quad (3.25)$$

where $x(t)$ is the signal and $H\{x(t)\}$ is defined as the Hilbert transform which is defined below

$$H\{x(t)\} = \frac{1}{\pi}\int \frac{x(t')}{t-t'}dt' \quad (3.26)$$

It is advantageous to convert the real signal to its complex analytic form because 1) if the real signal is used then positive and negative frequencies exist that will give rise to cross terms. By eliminating the negative frequencies we eliminate the cross terms 2) when using the analytic signal we require the first moment of the distribution to be the derivative of the phase which is the IF. Also, it allows the computation of the magnitude and phase of the signal so that the IF can be derived. 3) the analytic signal eliminates the need to sample at twice the Nyquist rate and 4) the analytical signal will provide an exact description of the average frequency

when using a real signal. The energy of the analytic signal is twice that of the energy in the real signal. The analytic signal can be viewed as putting the low frequency content in the amplitude and the high frequency content in the term $e^{j\phi(t)}$. There are several methods of computationally deriving the analytic signal. One implementation described by Boashash implements the Hilbert transform using a 79 point finite impulse response filter[Boa87]. Computationally, the analytical signal can be obtained by taking the FFT of the signal, zeroing the negative frequencies, multiplying the positive frequencies by two and then finally taking the inverse FFT.

Chapter 4

4 Assessment of the Time-Frequency Spectral Analysis Distributions using Simulated Heart Rate Variability Signals

4.1 Introduction

Only recently has the use of Cohens class of TF distributions been introduced as a potential clinical tool in the analysis of physiological signals. Until this time, the STFT has been used because of its ease of implementation[Van87][Dur90]. Other methods used in analyzing nonstationary signals include the running adaptive autoregressive algorithms. However the drawbacks of these methods include the inability to track transients, a priori knowledge in the selection of adaptive parameters and a suitable model order [Bia93]. Applications of TF methods include the use of the Wigner-Ville distribution in ECG analysis [Abe89]. Novak et al first introduced the application of the WD to HRV, blood pressure and respiration signals [Nov93]. Wang et al had applied the pseudo-Wigner (no time smoothing) distribution in impedance cardiography [Wan95]. Afonso et al has demonstrated the improved performance of the smoothed pseudo-Wigner over the STFT in the detection of ventricular fibrillation[Afo95]. In TF spectral analysis there is no method that can be considered optimum as the method is dependent on the particular signal class under analysis[Jon92]. It has been suggested that the ED or Choi-Williams

distribution, which belongs to a class of reduced interference distribution, may improve on the WD[Cho89]. Williams et al applied it to the EEG signal for epileptic patients and demonstrated its clinical viability[Wil95]. To the author knowledge, the SPWD and the ED have not been applied clinically to the HRV signal.

This chapter will compare and evaluate the performance of several TF distributions including the spectrogram, SPWD and ED using simulated nonstationary and stationary HRV signals. This is necessitated by the fact that in order for these distributions to be effectively used and interpreted as a viable clinical tool, the effects of the various parameters on the performance of the distributions must be understood. Issues such as IF tracking, cross term suppression, resolution(-3 dB bandwidth), frequency bias and variance will be examined. In addition, the SNR performance will be addressed as limited studies have addressed the noise performance or provided a comparative evaluation of these estimators.

4.2 Simulated HRV Signals

As mentioned in Chapter 2, a considerable amount of work has been done using traditional spectral analysis techniques tools such as the FFT and

autoregressive spectral estimation with the assumption of signal stationary in analyzing the HRV signal. These studies have shown that the HRV spectrum is generally characterized by the following:

a) narrowband signals that represent the various autonomic control mechanisms. The normal spectrum consists of 3 distinct peaks. Pathological or pharmacological induced conditions usually involve a compromise of one or two of the peaks.

b) signals that can be nonstationary and dynamic as the peaks shift in frequency. This is due to the underlying interaction of the physiological control systems. Attempts are made to conduct the recording under steady state conditions (rest conditions, minimal patient movement and fixed respiration), however this may not always be attainable.

In order to evaluate and compare the performance of the various TF distributions, consider the following simulated HRV signal noted below. The signal and its spectrum are shown in Figure 4.1

$$\begin{aligned} HRV(i) = {} & \{1+0.4\cos(2\pi*0.007*i)\}*\cos(2\pi*0.03*i)+ \\ & \sin\{(2\pi*0.1*i)+5\sin(2\pi*.007*i)\}+\cos(2\pi*(.2i+.0002i^2))+n(i) \end{aligned} \quad (4.1)$$

Venturi et al has cited this as a representative dynamic form of a HRV signal which was used to test various spectral estimators[Ven91]. The signal consists of frequency modulated, amplitude modulated and linearly modulated components. The first term of the signal is an amplitude modulated signal at the thermoregulatory peak (0.03 Hz). The second term consists of a frequency

modulated component at the blood pressure frequency (0.1 Hz) and finally the third component, a linearly modulated or chirp component that sweeps across the respiration frequencies (0.2-0.4 Hz). The term n(i) is an additive gaussian white noise term that is introduced to model physiological, transducer or electrode noise.

In addition, in order to examine in more detail the TF distribution statistical properties (variance and bias), they will be applied to a stationary representation of a HRV signal that consists of three sinusoid components with representative VLF, LF and HF HRV frequencies.

$$HRV(i) = \cos(2\pi * 0.03 * i) + \cos(2\pi * .1 * i) + \cos(2\pi * 0.3) + n(i) \qquad (4.2)$$

In the case of stationary analysis, the effect of the kernel on the time-indexed autocorrelation function which is defined in the next section will be examined to determine what impact it has on the variance and bias. In examining the SNR performance of the TF spectral estimators, simulations will be conducted under moderate (10 dB) and severe (5 dB) SNR levels. The SNR is defined as follows:

$$SNR = 10\log\left\{\sum_{i=1}^{N}|s(i)|^2 \Big/ \sum_{i=1}^{N}|n(i)|^2\right\} \qquad (4.3)$$

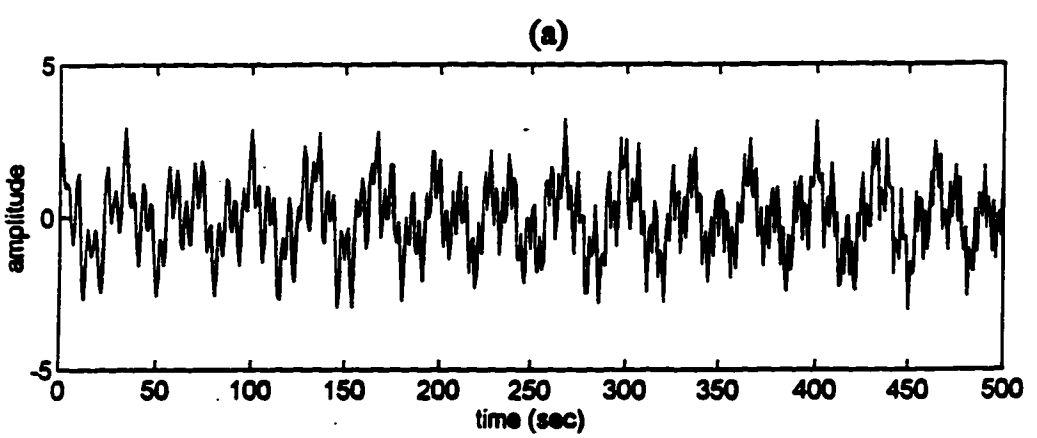

(b)

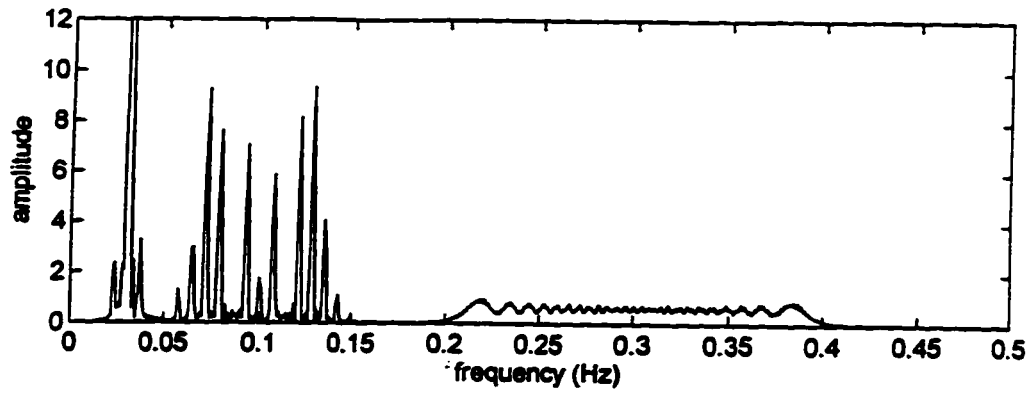

Figure 4.1 a) Simulated HRV signal with the frequency modulated, amplitude modulated and linear modulated signal classes b) Spectrum of the entire simulated HRV signal

4.3 Implementation of Cohens Class of Distributions

An unified definition of the Cohen class of distributions was proposed in section 3.2. In order to implement this in a discrete form[Boa90], the definition can be integrated with respect to θ to obtain

$$C(t,\omega) = \frac{1}{4\pi^2}\iint s^*(u-\frac{\tau}{2})s(u+\frac{\tau}{2})\Phi(t,\tau)e^{-j\omega\tau}\,du\,d\tau \qquad (4.4)$$

The discrete form of this equation can be written as

$$C(n,k) = \sum_{m=-L}^{L}\sum_{p=-P}^{P} s^*(n+p-m)s(n+p+m)\Phi(p,m)e^{-j4\pi mk/N} \qquad (4.5)$$

where $\Phi(p,m)$ is the kernel, $L=(N-1)/2$ (L is the data length), $P=(M-1)/2$ (M is the amount of time smoothing). The above equation can also be viewed as a follows:

$$C(n,k) = F_{m\to k}\{\Phi(n,m) * K(n,m)\} \qquad (4.6)$$

This is expressed as the Fourier Transform with respect to the lag m of the convolution (in the time domain) between the time-indexed autocorrelation function and the time-lag kernel $\Phi(n,m)$. The time-indexed autocorrelation function is defined as:

$$K(n,m) = \begin{cases} s^*(n-m)s(n+m) & for \quad m \geq 0 \\ K(n,-m) & for \quad m < 0 \end{cases} \qquad (4.7)$$

The general algorithm used to compute the SPWD and ED is shown in Figure 4.2. The mean DC components are removed prior to analyzing the data. In order to compute the TF distribution the analytic signal is computed as described in section 3.4. The analytic signal is zero padded at the front and end of the signal array so that no data is wasted in the computation of the algorithm. The kernel is generated next and due to symmetries only half the kernel is computed. The individual kernels for the SPWD and the ED are generated for $\Phi(n,m)$ and are shown in Figure 4.3. The time indexed autocorrelation products are computed next. This autocorrelation matrix is Hermitian therefore one can exploit this property so that the autocorrelation need only be computed for positive time lags therefore the summations in equation 4.5 can begin from 0. The other values are

computed from symmetry. In the case of the WD, the kernel is $\delta(t)$, so this convolution is not done.

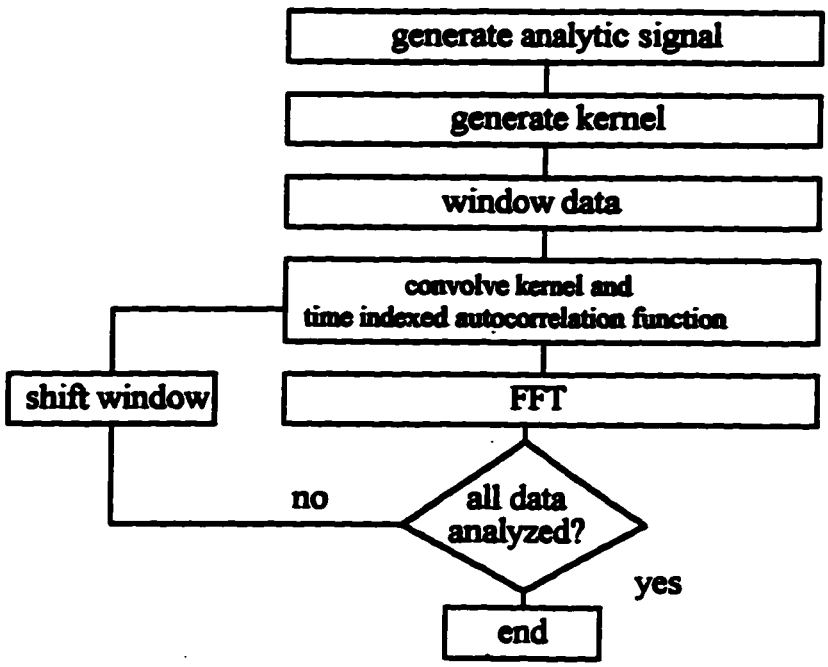

Figure 4.2. Flowchart of the computation of the TF distribution

The kernels are scaled so that the marginals are preserved. A 512 point FFT with zero padding is performed with respect to the lag. The frequency spacing of the TF distribution is $\Delta f=i/(2*\text{FFT length})$ because the entire frequency plane is used unlike the FFT where only have the frequencies are used. (i.e. The Cohen class distribution are periodic in π not 2π). As a result of the analytic signal being used only the positive frequencies need to be displayed. The observation window is then shifted by a specified amount and the aforementioned procedure is repeated.

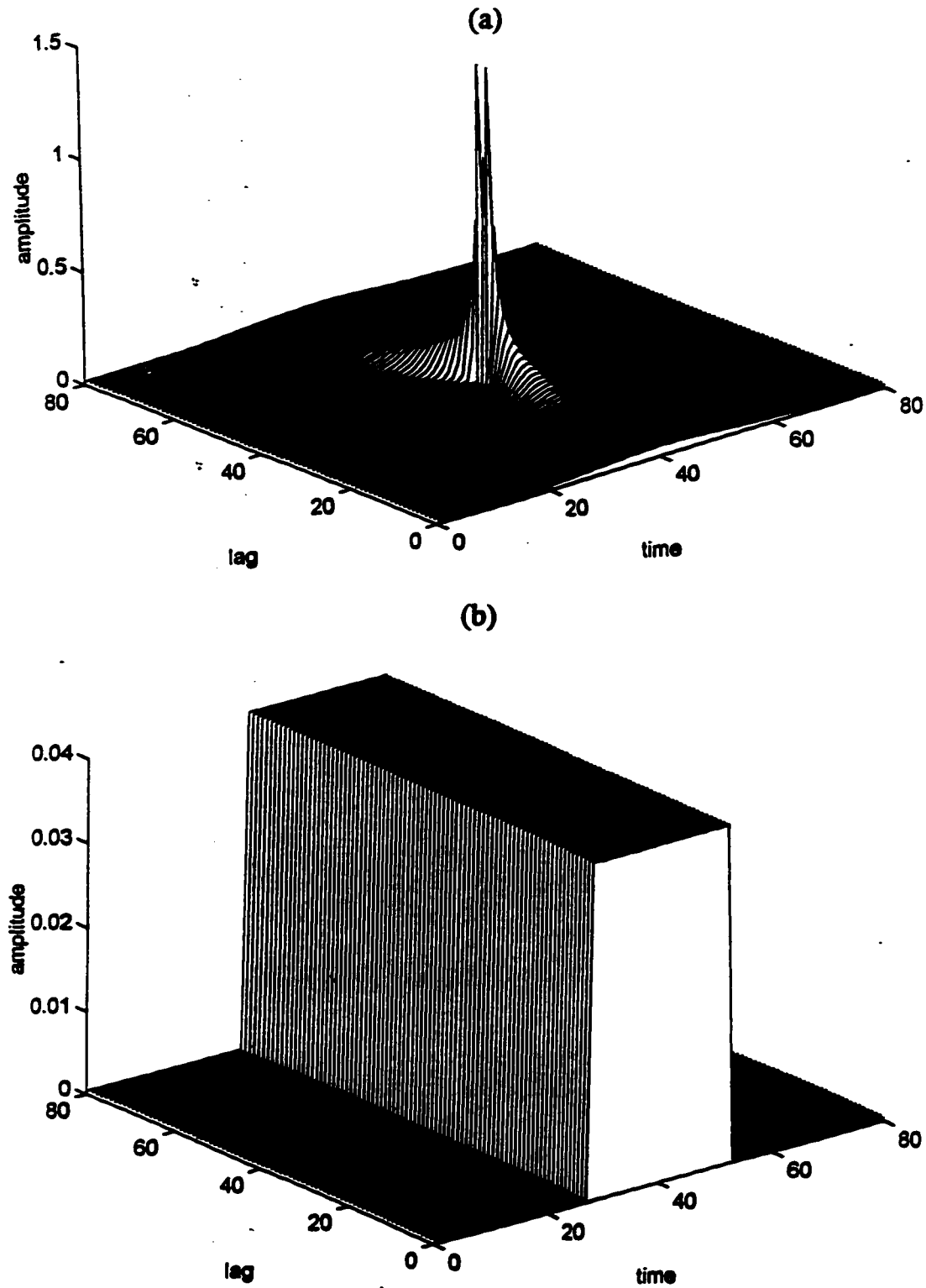

Figure 4.3 Kernels for the a) SPWD and b)ED

4.4 Short-Time Fourier Transform

The spectrogram (SPEC) which is the STFT magnitude squared has been a commonly used TF analysis tool because of it ease of implementation and is defined below.

$$STFT(n,k) = \sum_{m=0}^{N-1} x(m)w(n-m)e^{-j2\pi km/N} \qquad (4.8)$$

$$SPEC(n,k) = \frac{1}{N}|STFT(n,k)|^2 \qquad (4.9)$$

N is defined as the length of the window. A moving window $w(n-k)$ is applied to the signal which is assumed to be stationary in this interval. The spectrogram resolution is dependent on the data length and data window used. For a linearly modulated signal, the exact analytic expression for the optimal data length is given in equation 3.5. However, this length (N=71) results in smearing of the simulated baroreceptor frequency modulated signal as shown in Figure 4.4. Note the broadening of the spectral estimates which is a result of the uncertainty principle when a short data length (N=31 pts) is used. A compromise in the window length was 51 pts as it adequately represented these 3 signal structures. This data length will be used as a means of comparison for the other distributions. In order to improve sidelobe behavior, a Hamming window or cosine tapered window can be used. This is at the expense of mainlobe bandwidth. The resolution of the

rectangular window and the Hamming windows are given by .89/N and 1.3/N respectively[Har78]. Contour and waterfall plots using rectangular and Hamming windows are shown in Figures 4.4 and 4.7. It can be seen that the Hamming window gives a good representation of the IF at the expense of resolution. The STFT noise performance at a SNR=5 dB is shown in Figure 4.9. When using a rectangle window the estimator is unable to track the IF of the baroreceptor component. The use of a Hamming window does a better job in preserving the IF representation however its use must be weighed against the poorer resolution and interference with the LF amplitude modulated component.

In further examining the performance of the TF spectral estimators, the resolution (-3db bandwidth), frequency bias error and variance were examined using the stationary HRV test signal consisting of 3 sinusoids. Table 4.1 and Figure 4.8 provide a resolution comparison between the various spectral estimators based on the average of 35 realizations. The Hamming window provides the poorest resolution of all the TF estimators. The robustness of the FFT is demonstrated for the various SNR conditions. The frequency bias error is increased for the FFT with the largest errors originating for the VLF component as shown in Table 4.2. The variances of the FFT based methods for the rectangle and Hamming windows are shown in Figure 4.10. An improvement in the variance is noted with the Hamming window. Statistically, the variance of the FFT is known

to improve when using various windows at the expense of the bias and can be considered to be an inconsistent estimator (the bias and variance do not → 0 as N→∞) [Kay81]. In an attempt to improve on the STFT, the next section will consider more elaborate time frequency distributions.

(a)

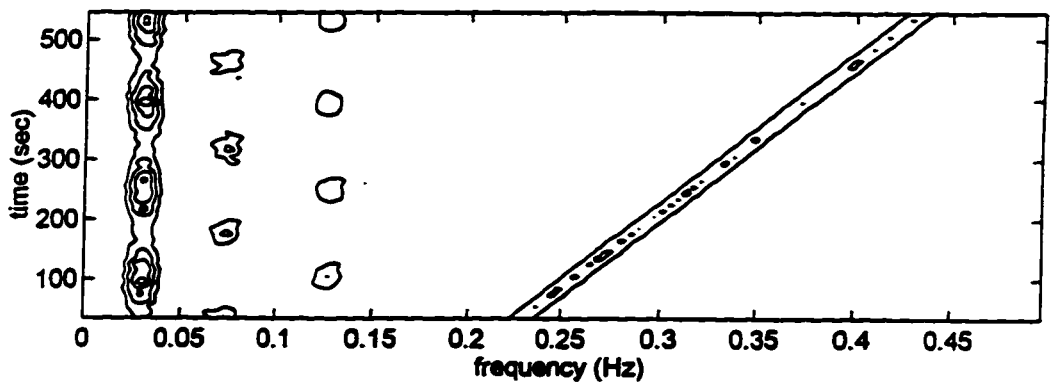

(b)

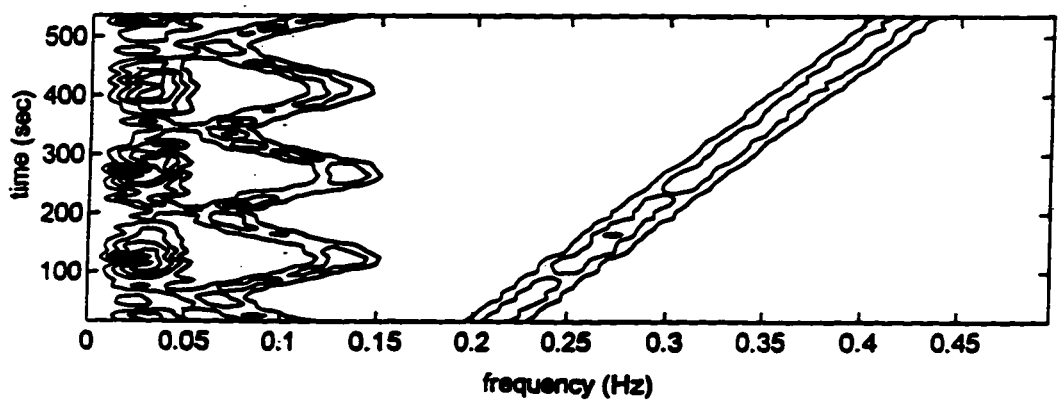

(c)

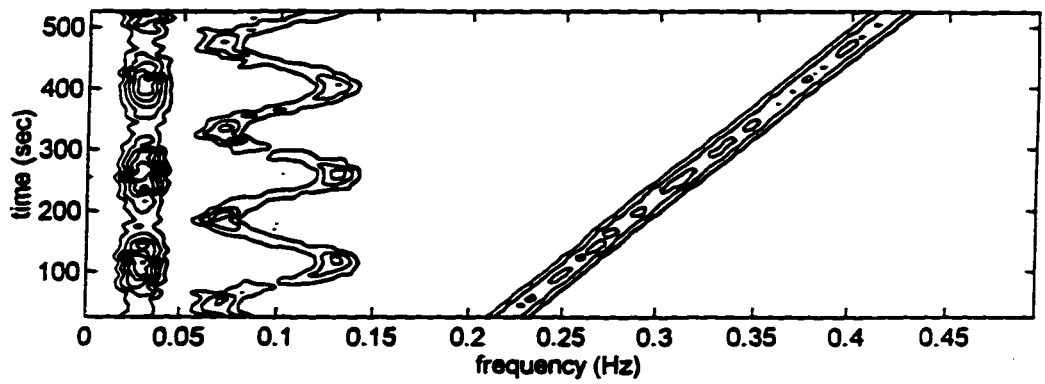

(d)

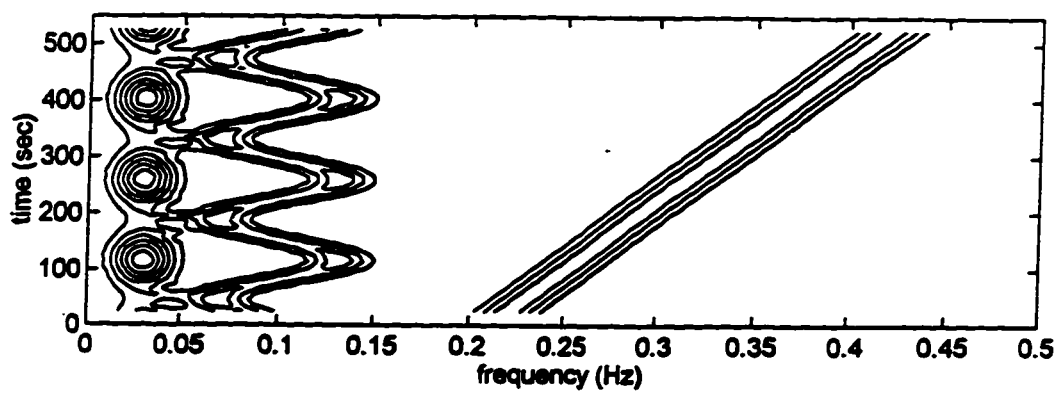

Figure 4.4 STFT contour plots a)N=71, rectangular window b) N=31, rectangular window c) N=51, rectangular window and d) N=51, Hamming window

4.5 Smoothed pseudo-Wigner Distribution

In order to improve on the STFT in terms of resolution and ability to track the IF, the discrete WD is introduced. As mentioned in section 3.3, the WD has a

kernel of 1. Using the HRV test signal, the WD contour and waterfall plots are shown in Figures 4.5 and 4.7. There are 3 cross terms that are obscuring the spectrum which is in agreement with Hlawatsch et al. who determined the number of cross terms to be N(N-1)/2 where N is the number of frequencies in the multicomponent signal [Hla92]. The amplitude of the oscillating cross terms at times is of greater amplitude than the autoterms. It can be seen that the WD offers both accurate representation of the IF and excellent resolution however cross terms plaque the interpretation of the spectrum. To suppress these cross terms, some degree of time and frequency smoothing maybe required. This leads to the practical implementation of the WD which is referred to as the SPWD as noted below:

$$SPWD(n,k) = 2\sum_{m=-L}^{L} |h(k)|^2 \left\{ \sum_{p=-P}^{P} g(p)s^*(n+p-m)s(n+p+m) \right\} e^{-j2\pi km/N} \quad (4.10)$$

g(p) is defined as the time smoothing window of length M. h(k) is defined as the frequency smoothing window. In the analysis of physiological signals, investigators have used gaussian and rectangular windows for frequency smoothing along with a rectangular window used for time smoothing [Nov93][Afo95]. In this manner, a rectangular window will be used for h(k) to achieve good resolution and the g(p) will be chosen as a rectangular window for time smoothing.

An important parameter in the use of the SPWD is choice of M which determines the degree of time smoothing or averaging need to suppress the cross terms in order to reveal the underlying signal structure. In another view, the choice of M should be as small as possible in order to approach the ideal resolution properties of the Wigner definition while at the same time being large enough to suppress cross terms. In the equation 4.10, when M=1 and h(k)=g(p)=1, the SPWD reduces to the WD. Figure 4.5 demonstrates the effect of M for a data length of 51 pts with g(p)=h(k)=rectangular window. It is noted in these simulations that generally little time smoothing is required to obtain the signal. With these simulated signals, a value of $M \cong N/2$ provides a good compromise between cross term suppression and time resolution. Full time smoothing (M=51) introduces the best condition in terms of cross term suppression however this is at the expense of resolution. In examining the SNR performance (5 dB) with M=23 it can be seen that the SPWD is able to provide better performance when compared to the STFT in tracking the IF as shown in Figure 4.9.

The effect of the M on the resolution is noted in Table 4.1 and Figure 4.8 using the stationary HRV signal. It is shown that with complete smoothing (M=51), the resolution approaches that of the FFT when using a rectangle window. As noted in Table 4.2, the SPWD frequency bias error is improved over the FFT. Figure 4.10 illustrates the decrease in the variance when increasing the

time smoothing. This result is consistent with Stankovic et al who demonstrated that in addition to suppressing the artifacts, noise signal improvements (making the variance finite) can be achieved by increasing the length of the time smoothing window at the expense of increasing of the bias[Sta93].

(a)

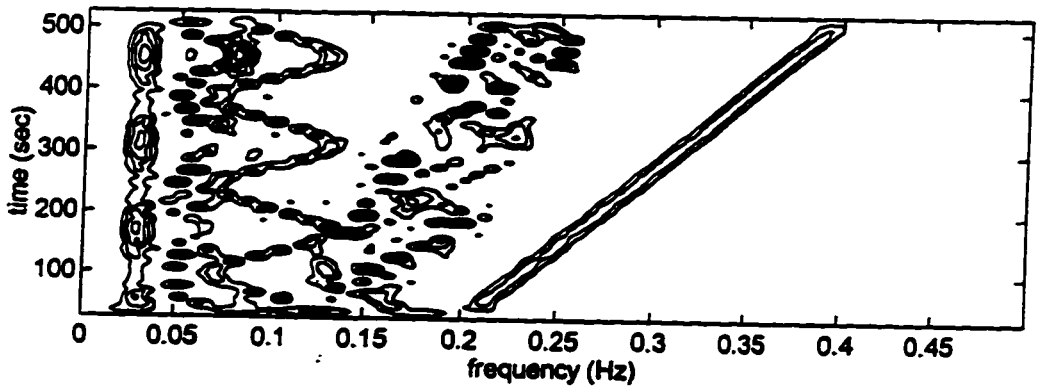

(b)

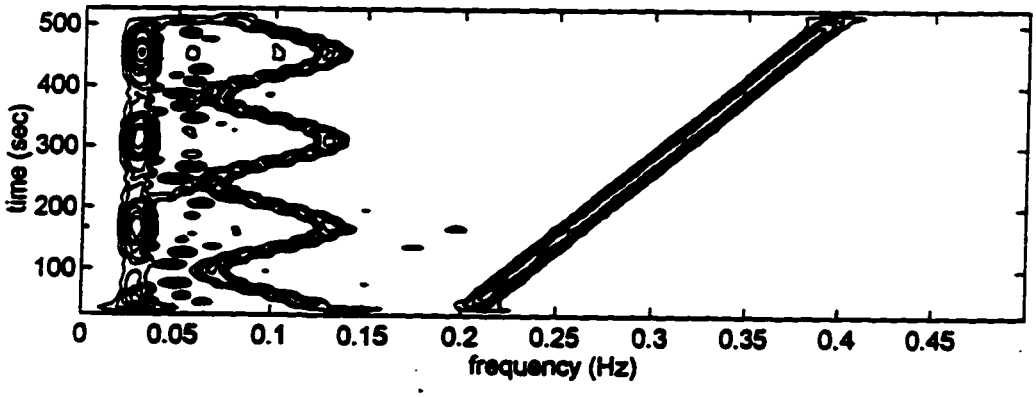

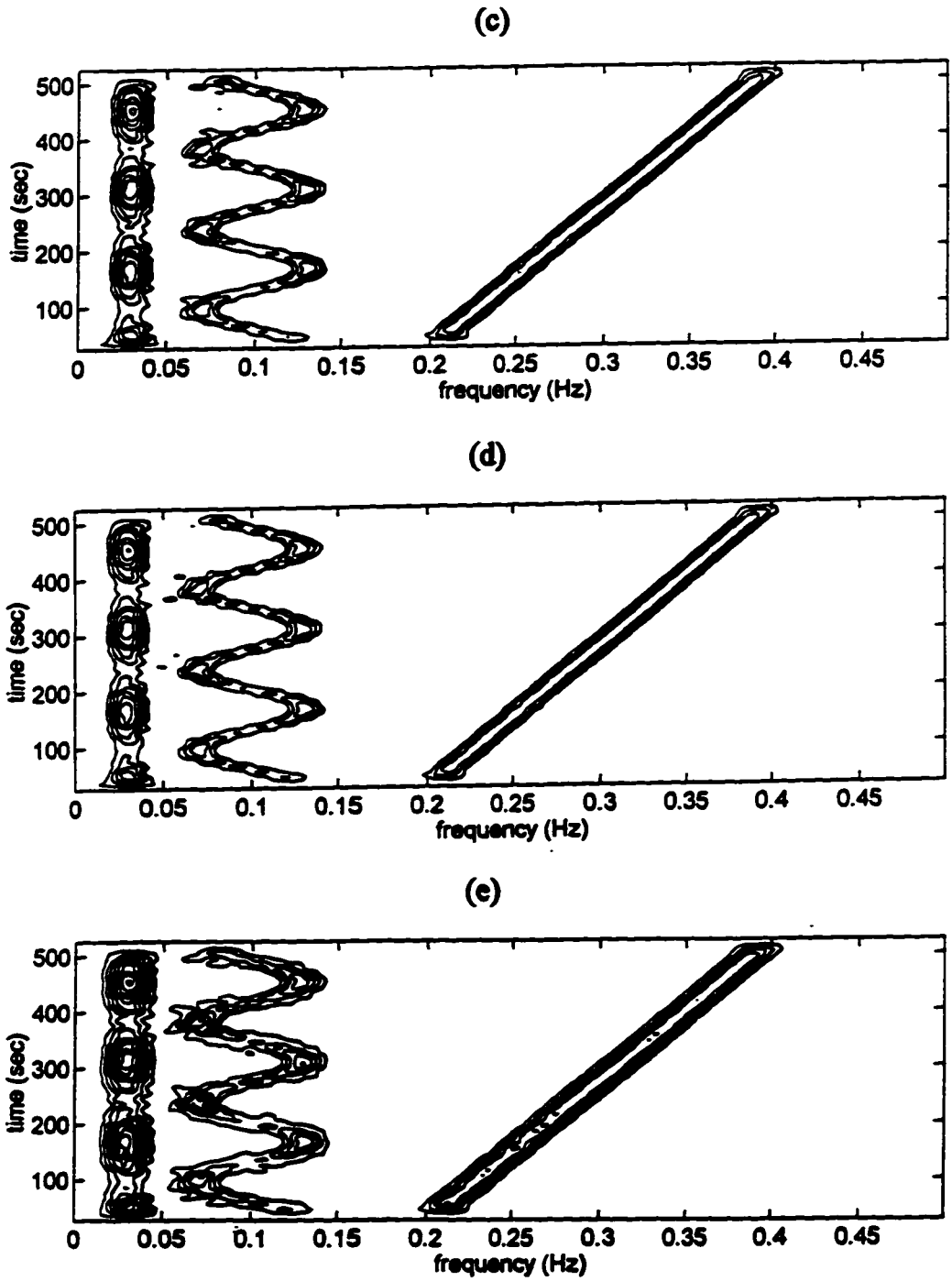

Figure 4.5 SPWD contour plots h(k)=g(p)=rectangular window a)M=1 b)M=11 c) M=23 and d) M=37 and e) M=51

4.6 Exponential Distribution

The ED was designed to minimize the effects of the cross terms and still satisfy the desirable properties of the WD. The discrete implementation of the ED is noted below.

$$ED(n,k)=2\sum_{m=-L}^{L}\left\{\sum_{p=-P}^{P}\sqrt{\frac{\sigma}{4\pi m^2}}e^{\frac{-\sigma p^2}{4m^2}}s^*(n+p+m)s(n+p+m)\right\}e^{-j2\pi km/N} \quad (4.11)$$

The ED allows for simultaneous time and frequency smoothing by the use of σ which must be carefully chosen to obtain good cross term suppression and resolution of the signal. Figure 4.6 demonstrates the effect of varying σ on the cross terms and on the autoterm resolution for N=51 pts. A value of $1 < \sigma < 5$ provided a good compromise between resolution and cross terms suppression. The contour plots of the ED are obscured by the smoothing characteristic of the kernel making the interpretation difficult. The ED offers better ability to track the IF than the STFT under no noise conditions however under the SNR=5 dB condition tracking the IF of the LF component is obscured as shown in Figure 4.7.

Table 4.1 and Figure 4.8 note the effect of σ on the resolution when using the stationary HRV signal. It is noticed that the ED approaches the WD as σ approaches ∞. It is seen that increasing σ allows for better frequency resolution with poorer cross term suppression. Decreasing values of σ result in poorer

resolution and approach that of the FFT (Hamming window). The ED frequency bias is similar to that of the SPWD. In examining the ED variance as shown in Figure 4.10, there is a slight decrease in the variance with decreasing σ.

(a)

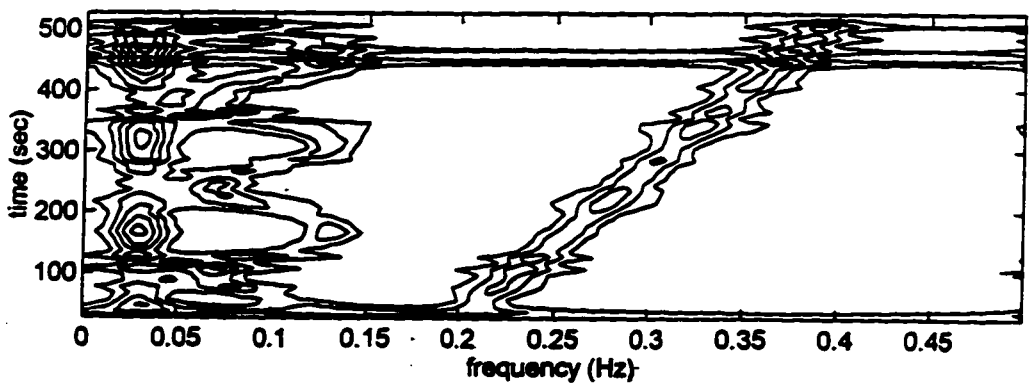

(b)

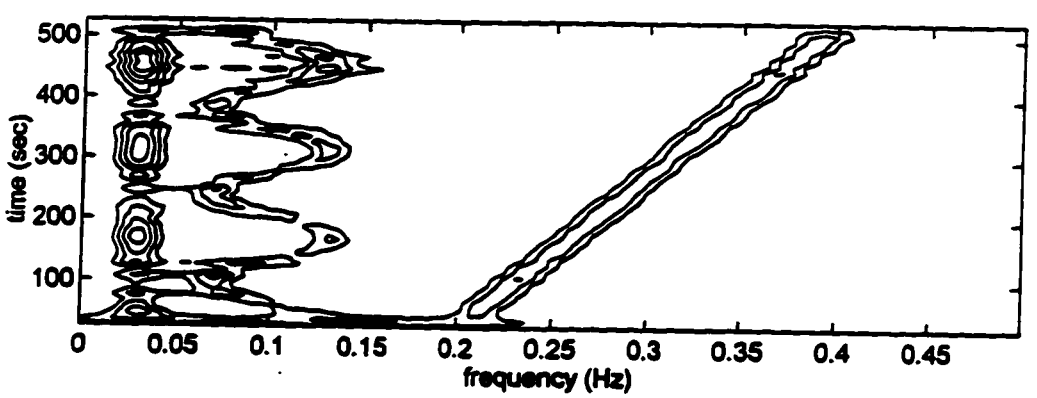

(c)

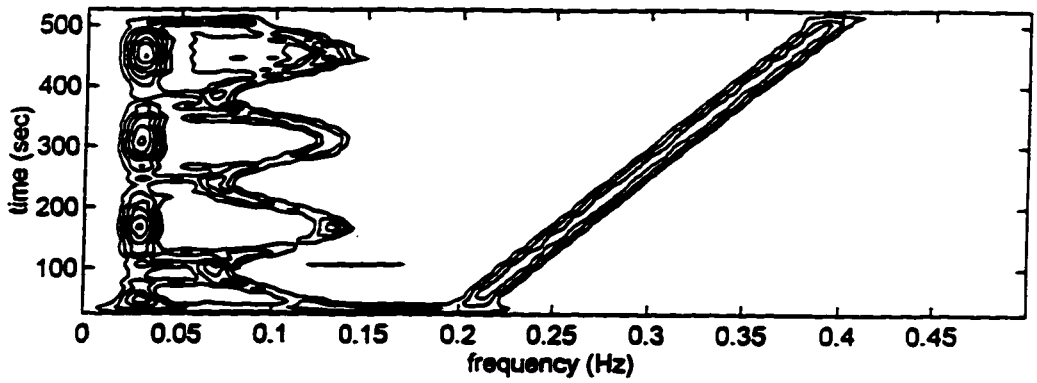

(d)

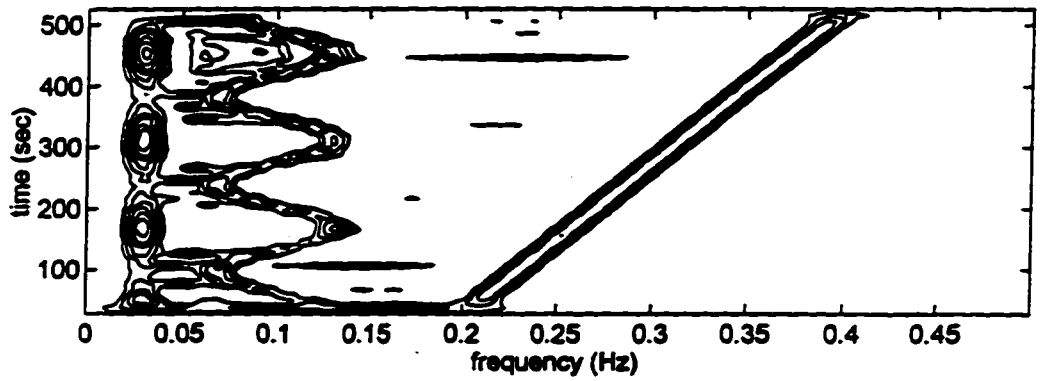

(e)

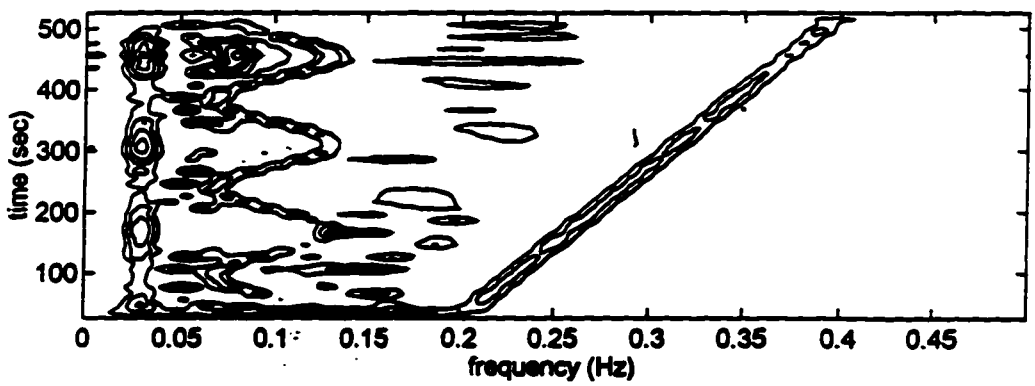

Figure 4.6 ED contour plots a)σ=.1 b) σ=1 c) σ=5 d) σ=10 and e) σ=100

(a)

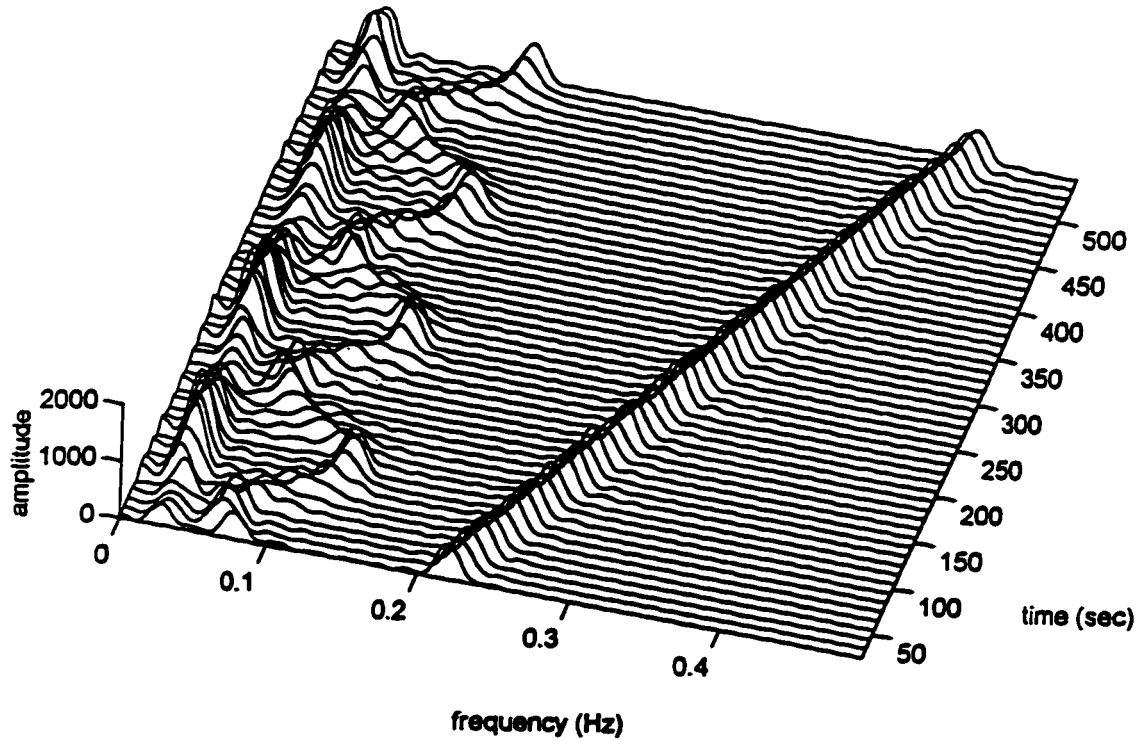
amplitude
2000
1000
0
0
0.1
0.2
0.3
0.4
frequency (Hz)
500
450
400
350
300
250
200
150
100
50
time (sec)

(b)

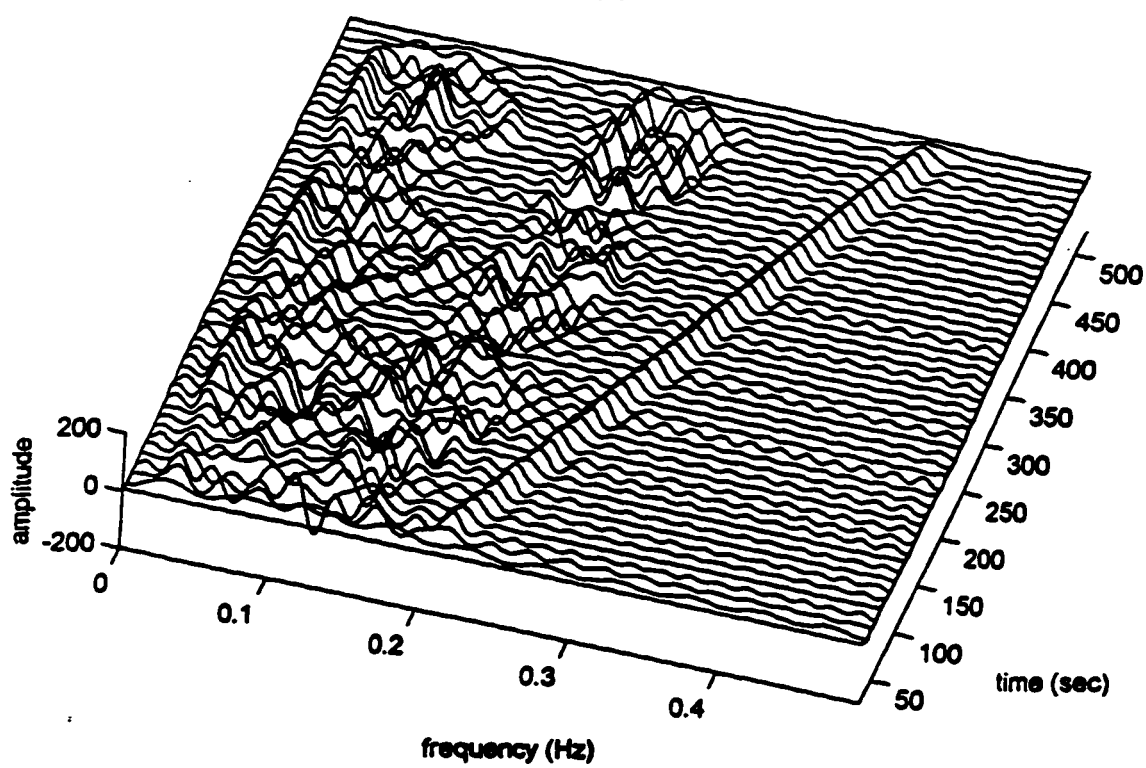
amplitude
200
0
-200
0
0.1
0.2
0.3
0.4
frequency (Hz)
500
450
400
350
300
250
200
150
100
50
time (sec)

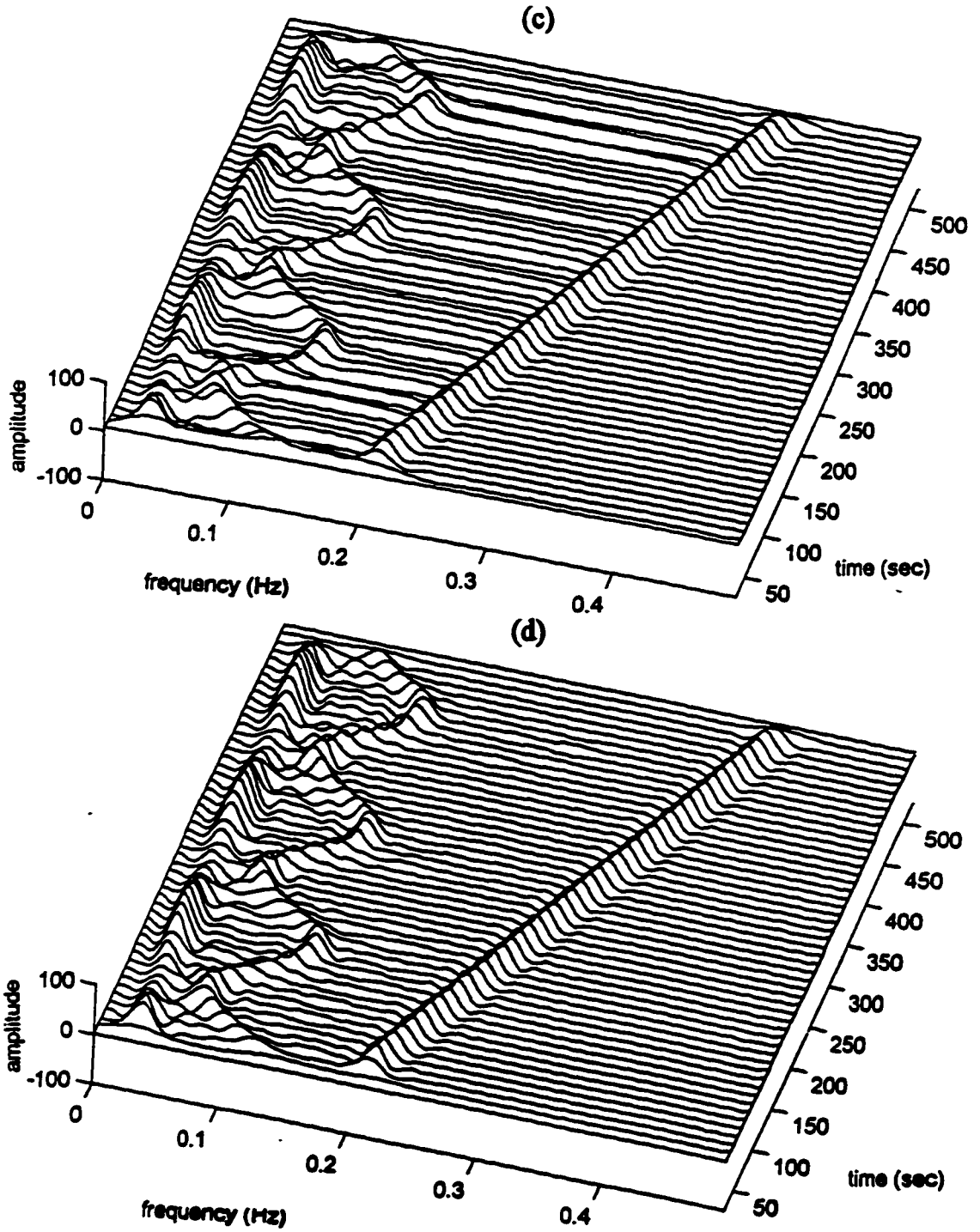

Figure 4.7 Waterfall plots of various TF distributions (N=51) a) STFT (rectangular window) b) WD c) SPWD (M=23, h(k)=g(p)=rectangular window) and d) ED ($\sigma = 5$)

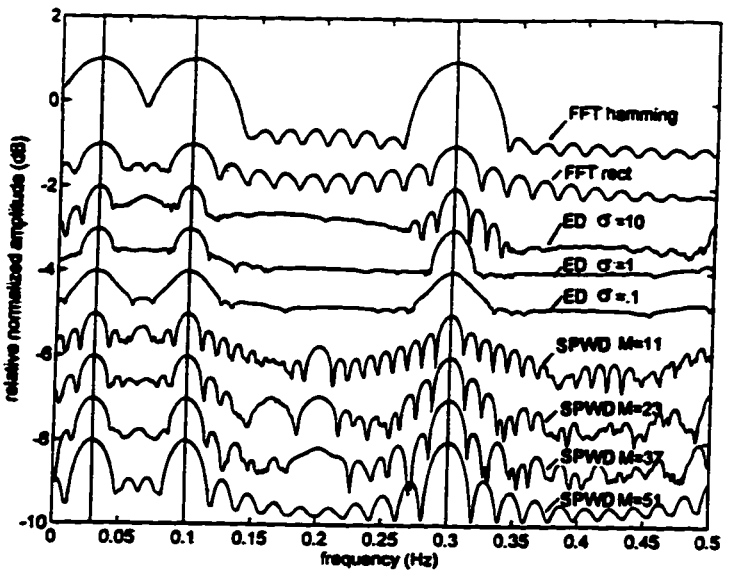

Figure 4.8 Resolution comparison of the various TF spectral estimators based on the average of 35 realizations under no noise conditions

(a)

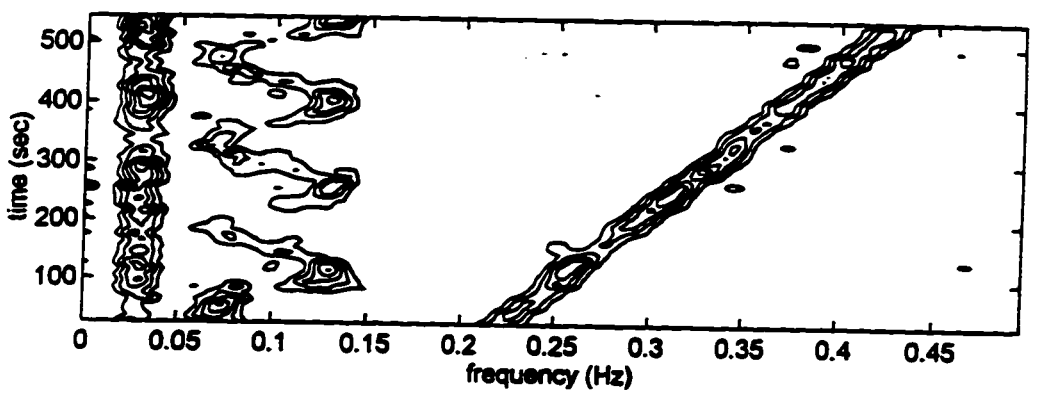

(b)

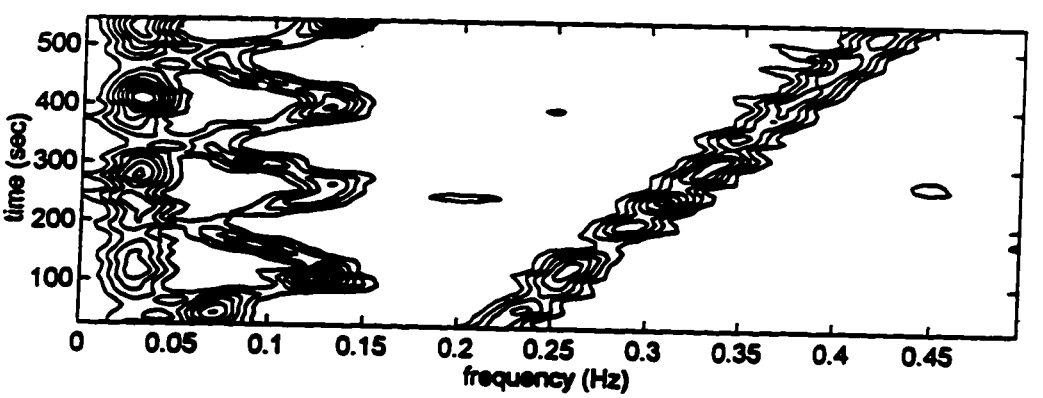

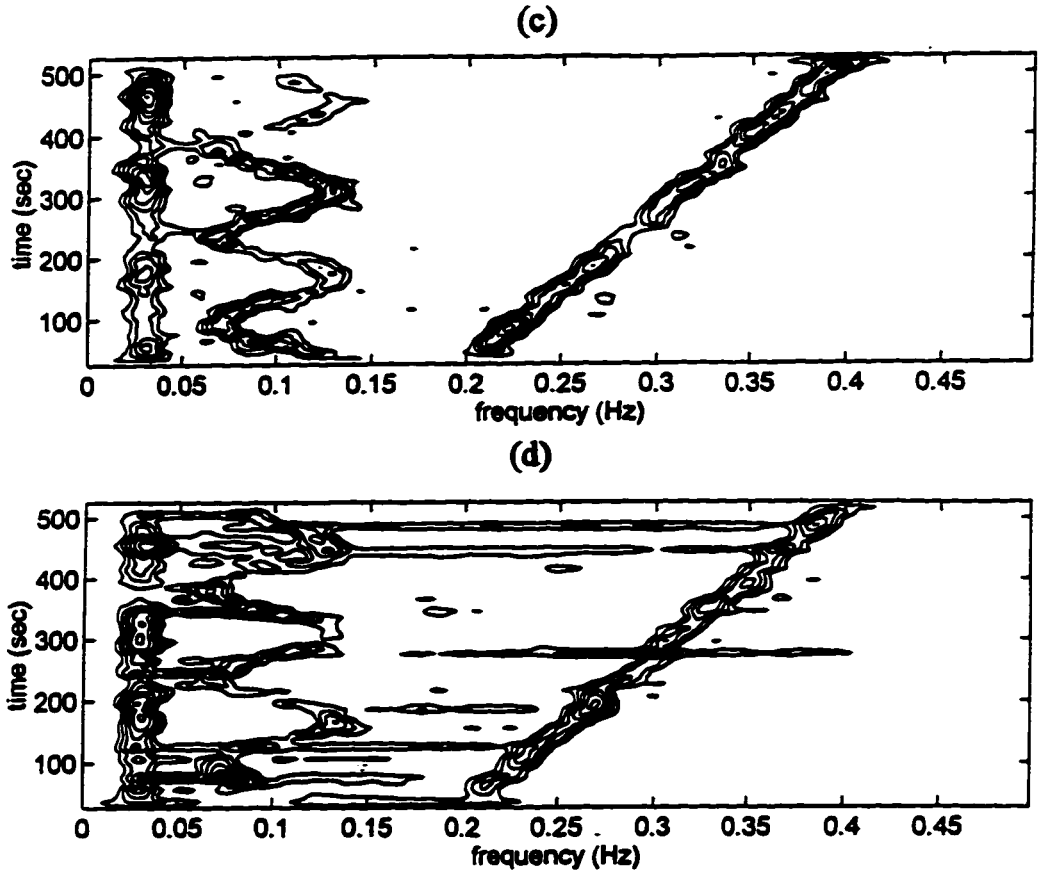

Figure 4.9 Effect of noise on the TF distribution contour plots, SNR=5 dB, N=51 a) STFT (rectangular window) b) STFT (Hamming window) c) SPWD (M=23) and d) ED ($\sigma = 5$)

Table 4.1. Resolution comparison of the various TF spectral estimators under no noise, SNR=10 dB and SNR=5 dB conditions

Spectral estimator	Resolution (Hz)		
	(no noise)	(SNR=10 dB)	(SNR=5 dB)
FFT (rect)	0.01746	0.01745	0.01762
FFT(hamm)	0.02557	0.02609	0.02571
SPWD (M=11)	0.01295	0.01304	0.01181
SPWD (M=23)	0.01509	0.01468	0.01381
SPWD (M=37)	0.01607	0.01658	0.01619
SPWD (M=51)	0.01660	0.01722	0.01695
ED(sig=.1)	0.02590	0.02556	0.02562
ED(sig=1)	0.01905	0.01848	0.01886
ED(sig=10)	0.01486	0.01481	0.01352

* resolution reported for the 0.3 Hz HF component

(a)

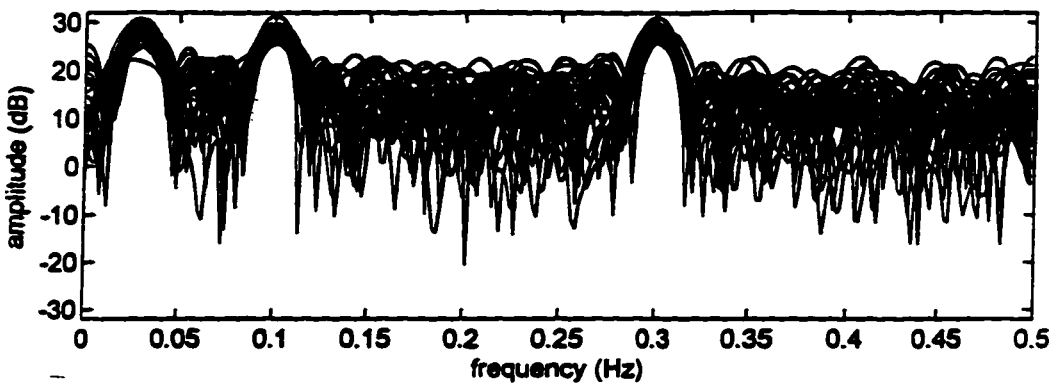
amplitude (dB)
30
20
10
0
-10
-20
-30
0
0.05
0.1
0.15
0.2
0.25
0.3
0.35
0.4
0.45
0.5
frequency (Hz)

(b)

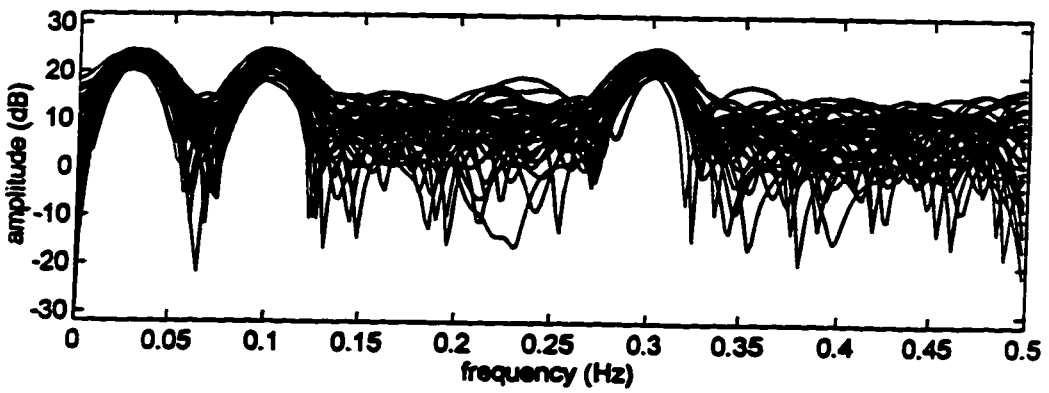
amplitude (dB)
30
20
10
0
-10
-20
-30
0
0.05
0.1
0.15
0.2
0.25
0.3
0.35
0.4
0.45
0.5
frequency (Hz)

(c)

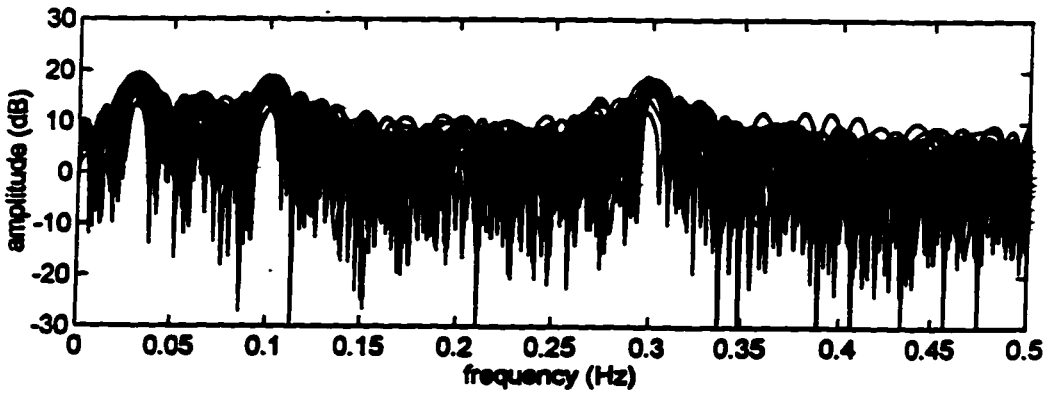
amplitude (dB)
30
20
10
0
-10
-20
-30
0
0.05
0.1
0.15
0.2
0.25
0.3
0.35
0.4
0.45
0.5
frequency (Hz)

(d)

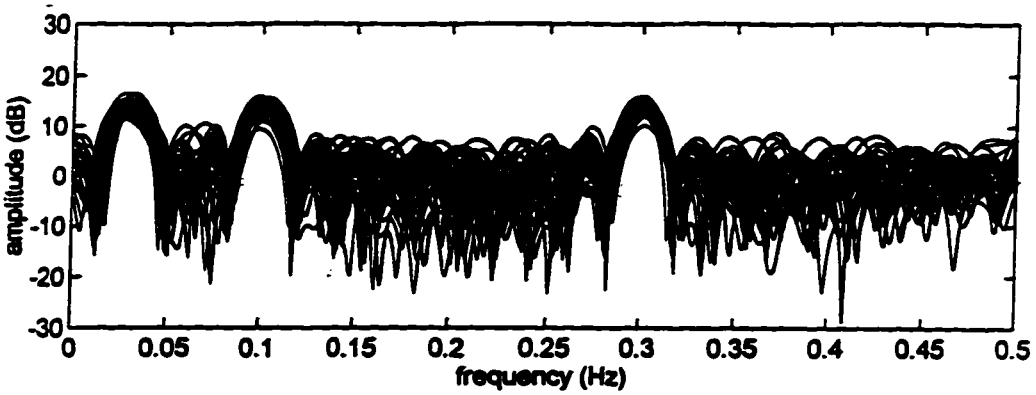

(e)

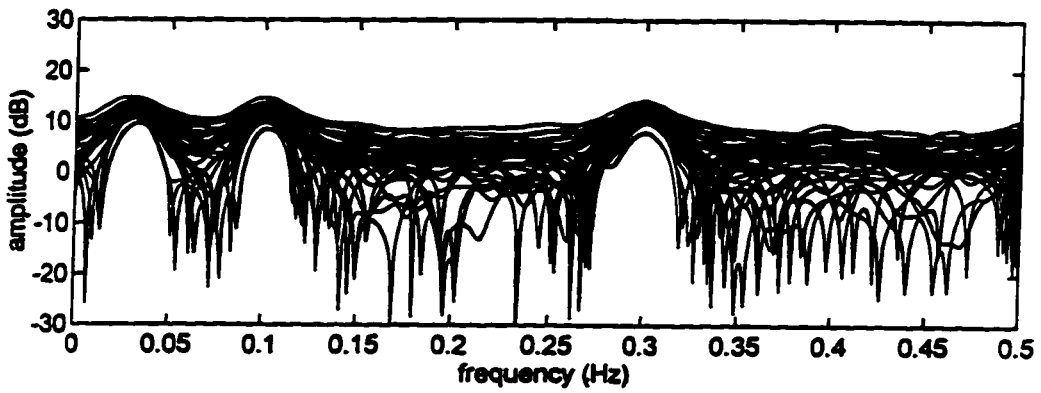

(f)

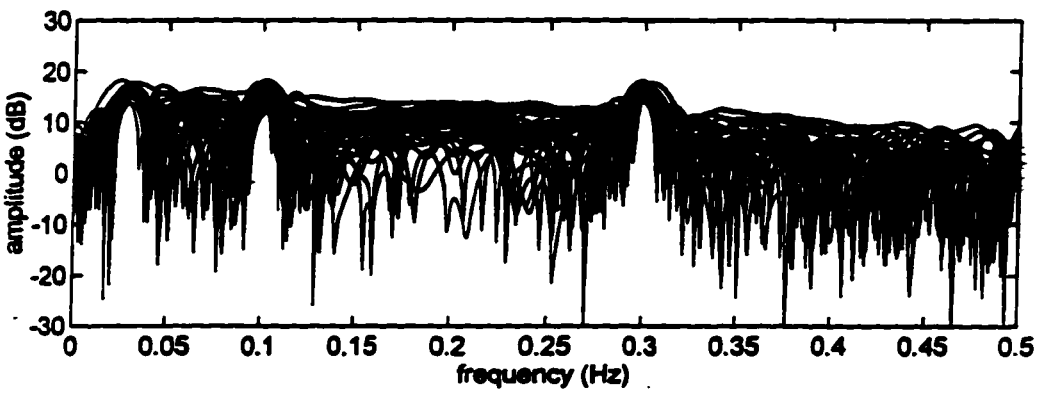

Figure 4.10 Variance comparison of the various TF estimators (35 overlaid realizations) SNR=5 dB a) FFT(rectangle window) b) FFT(Hamming) c) SPWD (M=11) d) SPWD (M=51) e) ED (σ =.1) and f) ED (σ = 10)

Table 4.2. Frequency bias error for the various TF estimators

	VLF peak			LF peak			HF peak		
	no noise	SNR= 10 dB	SNR= 5 dB	no noise	SNR= 10 dB	SNR= 5 dB	no noise	SNR= 10 dB	SNR= 5 dB
FFT (rect)	6.3%	7.3%	7.0%	1.9%	2.1%	2.2%	0.7%	0.6%	0.5%
FFT(hamm)	5.0%	7.0%	3.7%	1.6%	2.2%	2.5%	0.8%	0.6%	0.6%
SPWD (M=11)	3.7%	3.3%	1.0%	1.0%	1.1%	0.3%	0.3%	0.4%	0.3%
SPWD (M=23)	3.7%	3.7%	2.7%	1.0%	1.0%	0.8%	0.3%	0.3%	0.4%
SPWD (M=37)	3.3%	3.7%	4.0%	0.9%	0.6%	0.7%	0.3%	0.3%	0.1%
SPWD (M=51)	3.3%	3.0%	3.7%	1.0%	0.8%	1.1%	0.3%	0.3%	0.4%
ED(sig=.1)	3.7%	3.3%	4.3%	0.9%	0.9%	0.6%	0.3%	0.3%	0.5%
ED(sig=1)	3.7%	4.0%	3.3%	1.0%	0.9%	1.1%	0.3%	0.4%	0.4%
ED(sig=10)	4.0%	2.7%	4.6%	0.8%	1.0%	0.6%	0.3%	0.3%	0.5%

4.8 Summary

A comparative study of the STFT, SPWD and the ED distributions was conducted using nonstationary and stationary simulated HRV signals.

The SPWD and the ED were able to adequately track the IF of the frequency modulated LF and linearly modulated HF components of the simulated HRV signal with good resolution. From the WD definition the exact expression of the IF can be obtained. In the ED we approach this expression for $\sigma \rightarrow \infty$. In the STFT, an approximation is obtained as a suitable data window cannot be chosen to attain this conditional average.

A resolution comparison has demonstrated the improved resolution properties of the SPWD (for small M) and the ED (large σ) over the STFT. However, the choice of M and σ must be judiciously chosen so that the tradeoff of

cross terms suppression and good resolution is achieved. For this simulated HRV signals, the adequate cross term suppression was achieved with $M \cong N/2$ for the SPWD and $1 < \sigma < 5$ for the ED. The statistical properties of these estimator have been studied and it is noted that the variance is improved with increasing M and decreasing σ. The variance of these methods are comparable to that of the STFT however these methods offer an improved frequency bias over the STFT. The robustness of these methods under various SNR conditions has been illustrated.

In general, this study has shown that the SPWD and ED offer a suitable alternative over the STFT in the analysis of nonstationary and stationary signals. Guidelines on the use of these distributions have been presented which will be used for the next chapter which will focus on a clinical application of these TF distributions on HRV signals.

Chapter 5

5. Application of Time-Frequency Spectral Analysis of Heart Rate Variability Signals to study the effects of Unilateral Stellate Blockade

5.1 Introduction

Blockade of the sympathetic chain has been used for many years for the control of chronic pain. It is desirable that this blockade does not affect modulation of HR as loss of sympathetic tone can lead to autonomic imbalance that could be fatal to the patient. In these patients that undergo right stellate blockade some impact on the HR is expected especially from those sympathetic efferents innervating the SA node. TF spectral analysis provides a tool to assess the degree of the stellate block. Other studies have suggested that there are no significant effects of unilateral stellate blockade on HR, systolic blood pressure or left ventricular ejection fraction at rest or during exercise[Joh87]. Subtle effects were however noted on QT interval under the stress of upright posture or exercise. As mentioned in Chapter 2, the distribution of post ganglionic sympathetic nerves to the heart is complex and variable in primates. Cardiac sympathetic fibers may originate, not just in the left or right stellate ganglia, but also from higher cervical ganglia. Sympathetic fibers are not necessarily unilateral and may cross from one sympathetic chain to the opposite side of the heart. Accordingly the effects of

unilateral stellate blockade on the heart may depend on the proportion of sympathetic outflow which passes through that stellate ganglion for each side of the heart. It is expected that the HR would be influenced largely by sympathetic fibers reaching the SA node. If nerve traffic in some of these fibers is interrupted by stellate blockade one would expect less influence of sympathetic activity on the SA node and HR. Sympathetic influences on the HR are understood to be limited to a frequency range of 0.05-0.15 Hz in the HR power spectrum [Pom85]. Therefore under sympathetic blockade a reduction of the power in this range is expected. The HRV spectrum of post stellate blockade patients was examined to look for the effects of this partial sympathetic blockade on the sympathetically mediated range of HRV.

5.2 Clinical Protocol and Data Acquisition

This study was conducted on seven patients aged 25 to 61 who were undergoing right stellate ganglion blockade for the control of chronic pain. Xylocaine or marcaine was injected in the region of the stellate ganglion. The presence of blockade was confirmed by all of the following: (1) a change in the temperature of the extremity (2) Horner's syndrome (3) absences of sweating on the blockaded side. Approximately 1-2 minutes of continuous instantaneous HRV signal was derived from the ECG recording using the method of inverse intervals.

Recordings were taken for both the supine and standing positions immediately before and two hours after the blockade procedure. The HRV signal was subsequently digitally low pass filtered at 1 Hz using a 10th order Butterworth filter. The effective sampling rate was 3 Hz. As determined from Chapter 4 an equivalent of 51 seconds was used for the data window. In addition for some patients, an impedance respiration signal was recorded using Healthdyne apnoea-bradycardia monitor. Representative HRV signal and respiration signals are shown in Figure 5.1. The data was examined with the use of the paired Student t-test (two-tailed). A p-value < 0.05 was considered significant. Prior to analysis, linear trends and the signal mean were removed from the signal. TF spectral estimates were generated using the SPWD and ED and are displayed using waterfall plots and contour plots to visually access the autonomic tone. In order to circumvent the issue of negative values in the TF distribution, it was decided to use the mean peak amplitude instead of the mean area under the predefined frequency bands. Finley et al. has shown that a linear correlation exists in using the areas and the peak values in each frequency band when using FFT based spectral analysis[Fin87]. Measures of the sympathetic and vagal tone consists of measuring the average baroreceptor amplitude in the LF frequency band (0.05-0.15 Hz) and the average respiration amplitude in HF frequency band (0.15-0.4 Hz). In addition, the LF/HF ratio will be computed which has been defined as an acceptable measure of the

sympathovagal balance[Pag86]. Increased values for the ratio suggest predominance of sympathetic activity.

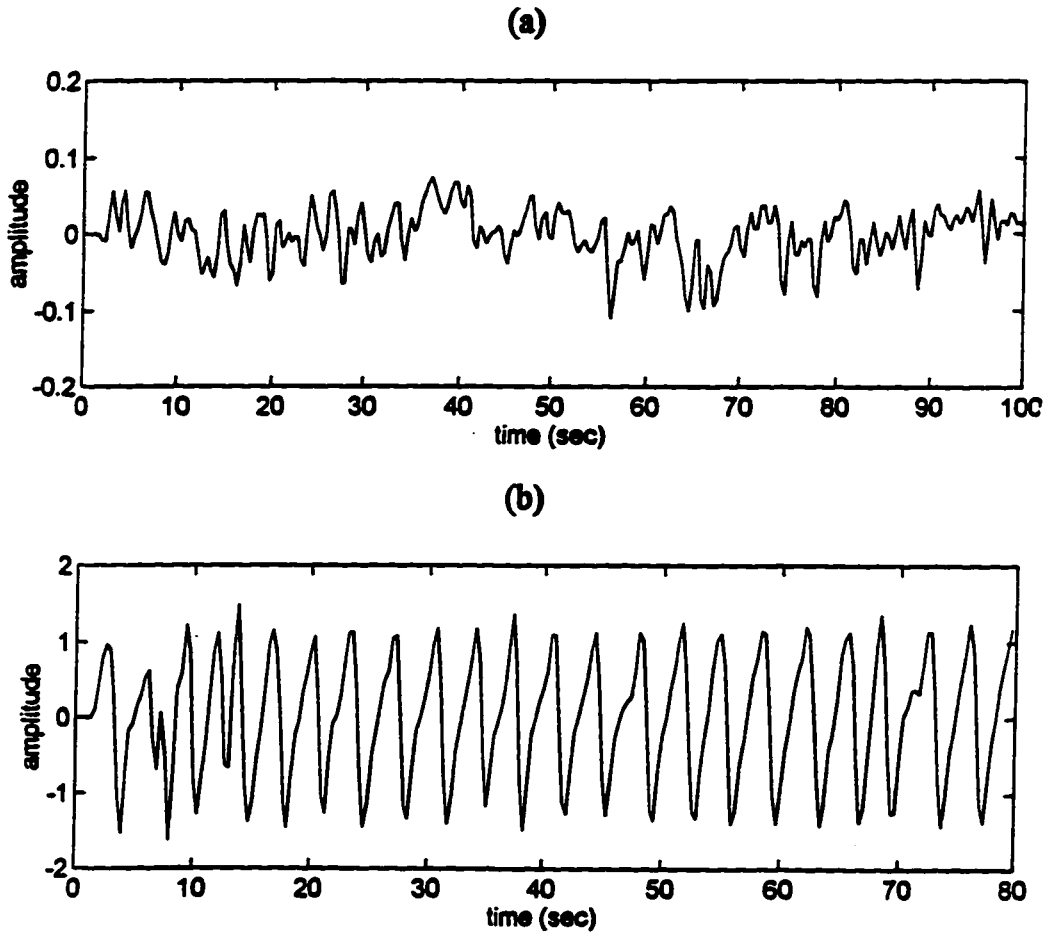

Figure 5.1 Representative a) HRV and b) respiration signal (mean respiration frequency = 0.28 Hz)

5.3 Results

The SPWD and ED were applied on the pre block and post block HRV patients under supine and orthostatic conditions. Using the guidelines for parameter selection for these distributions from chapter 4, a subset of the pre block and post block patients were used to establish the adequate performance of the distributions. Figure 5.2 illustrates the SPWD (h(k)=g(p)=rectangle window, M=N/2) and ED (σ=1) TF spectrum for a pre block patient (mt) in the supine position. These distributions illustrate the presence of the VLF, LF and HF peaks. By recording the respiration signal, its presence and frequency is confirmed in the HRV TF spectrum. In comparing the contour plots, the SPWD was noted to be a better tool in separating out the components when compared to the ED. The smoothing characteristic of the exponential kernel obscures the contour spectrum. In general, the recordings of these patients were of short duration and were able to be recorded under steady state condition. This resulted in a relatively fixed frequency location of the VLF, LF and HF components. It is also noted that these TF plots are characterized by harmonic frequencies. There is evidence to suggest that autonomic modulation at the SA node is a pulse frequency modulation process for which multiples of the VLF, LF and HF frequencies may exist in the spectrum[deB85]. The components were sufficiently removed from each other and if required time smoothing could be increased to smooth out these harmonics as

well as extraneous noise without affecting the interpretation of the TF spectrum. This is at the expense of poor autoterm resolution and increased computational load. It should be noted that full time smoothing also results in attaining a positive distribution. This approach is useful if integration of areas under the predefined frequency bands is desired.

SPWD of the HRV signal

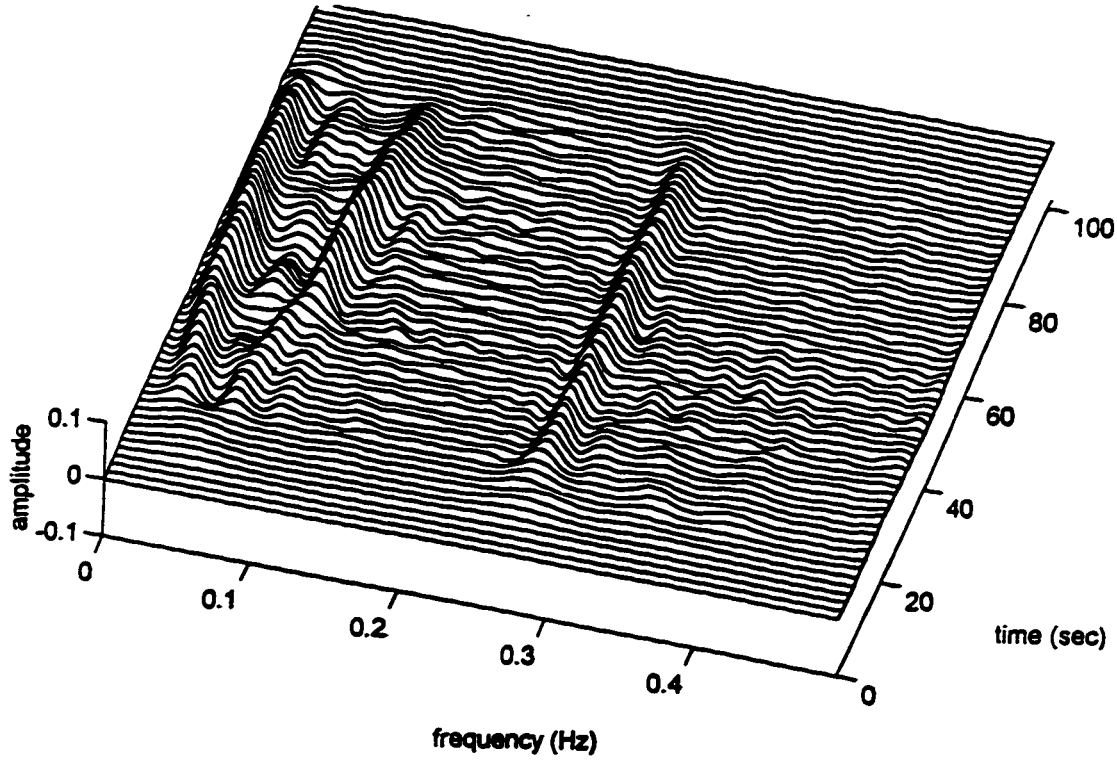

ED of the HRV signal

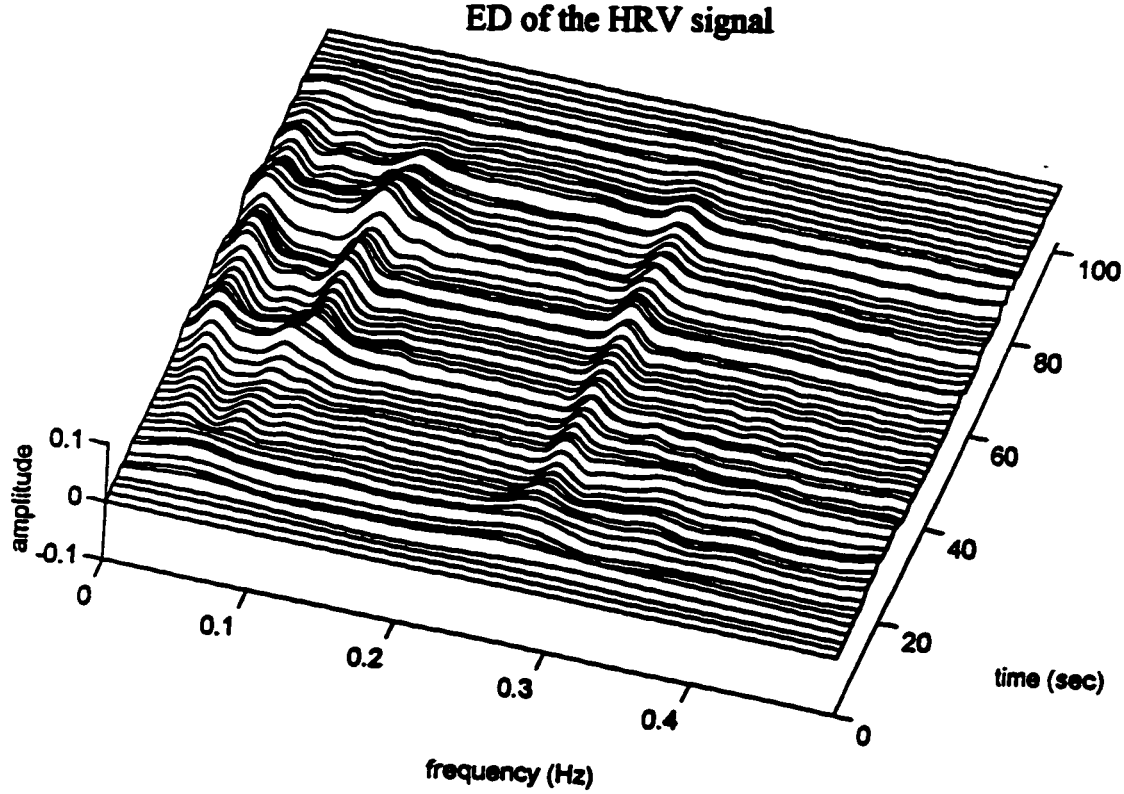

SPWD of the respiration signal

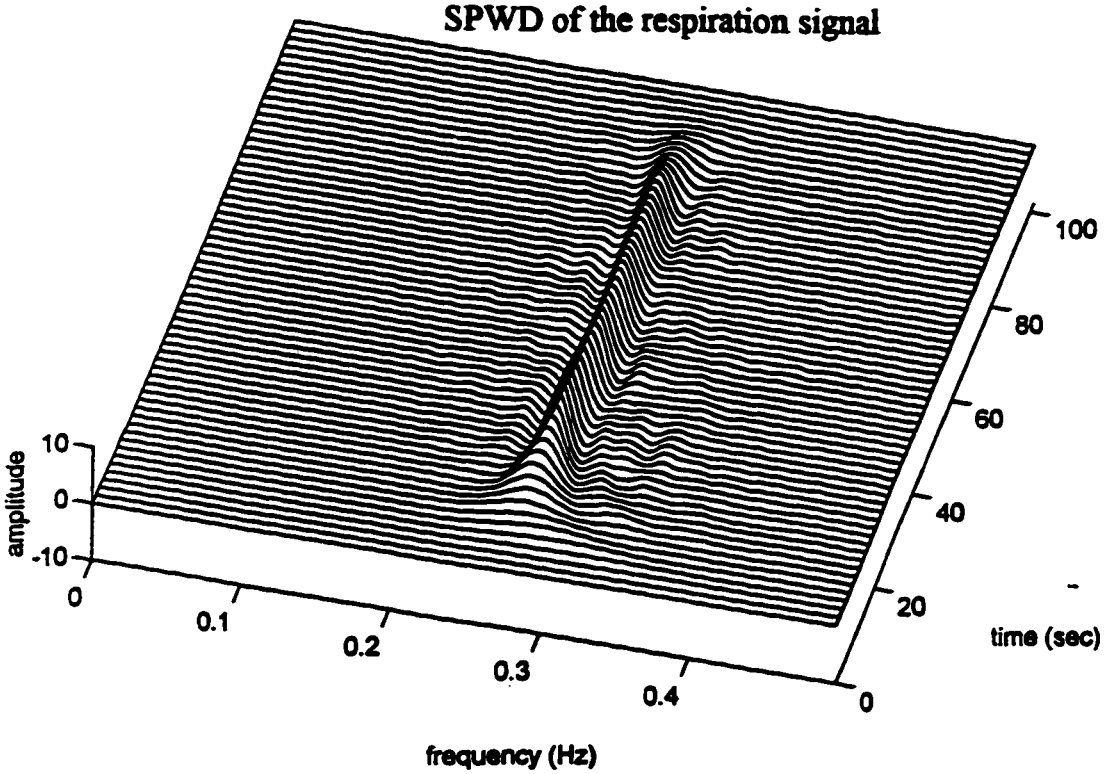

SPWD of the HRV signal

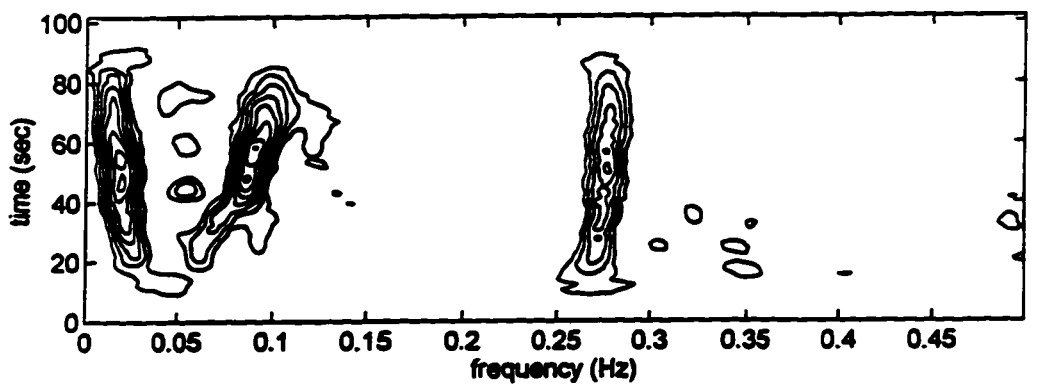

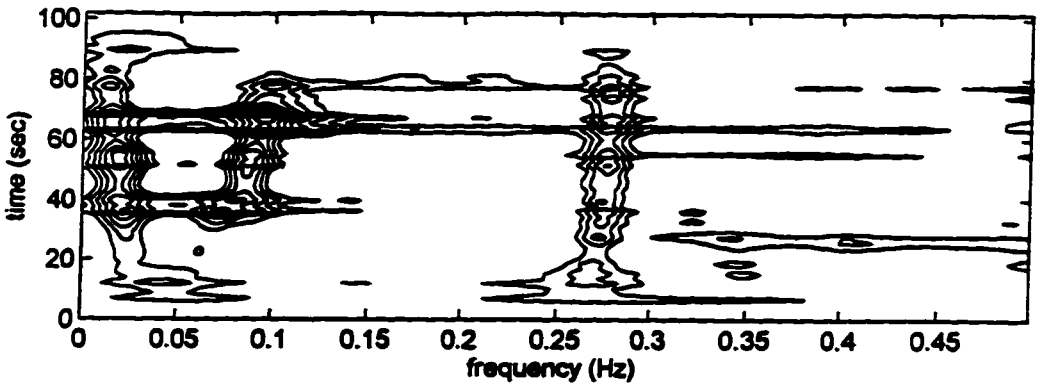

Figure 5.2 TF waterfall and contour plots for a pre block patient (mt) in the supine position using the SPWD (h(k)=g(p)=rectangle window, M=N/2), ED (σ=1) and SPWD of the respiration signal.

Figure 5.3 illustrates the effect of orthostatic stress on the HRV spectrum (SPWD and ED) from the supine to standing position under pre block conditions. Under orthostatic stress the LF component is increased which is consistent with work from other investigators[Pom85][Nug86]. In the supine position the HF component is increased.

SPWD supine

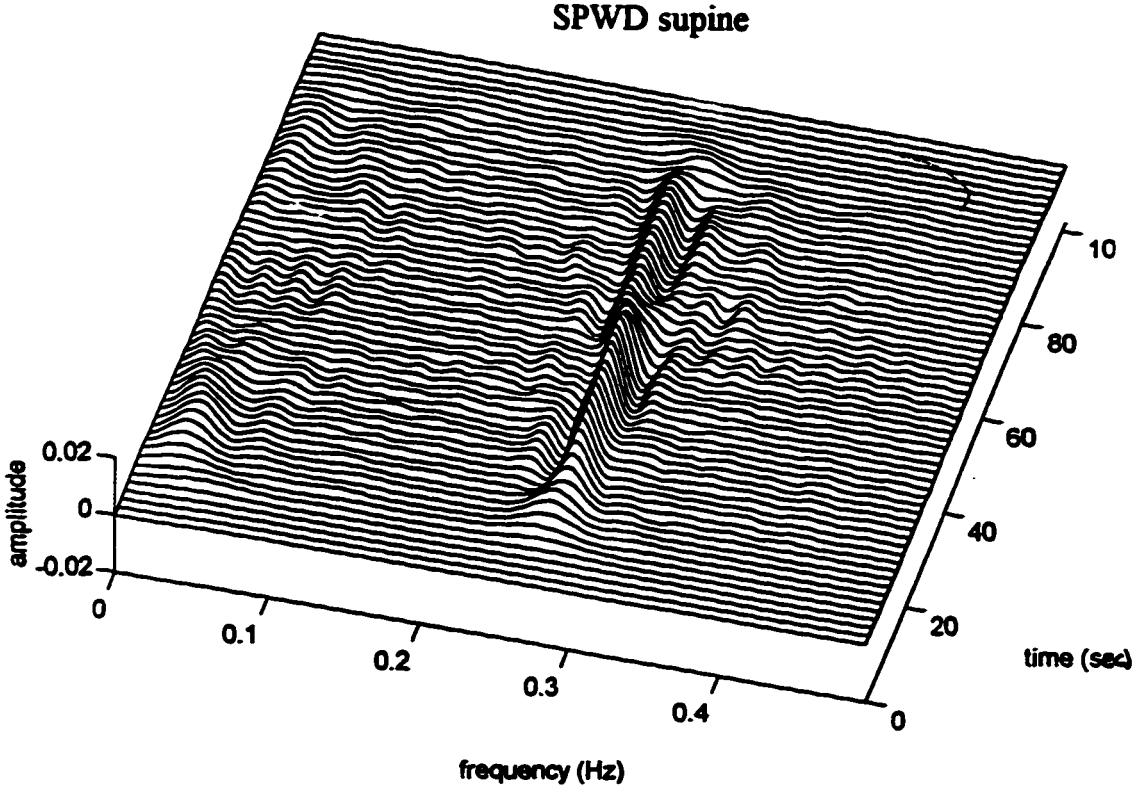

SPWD standing

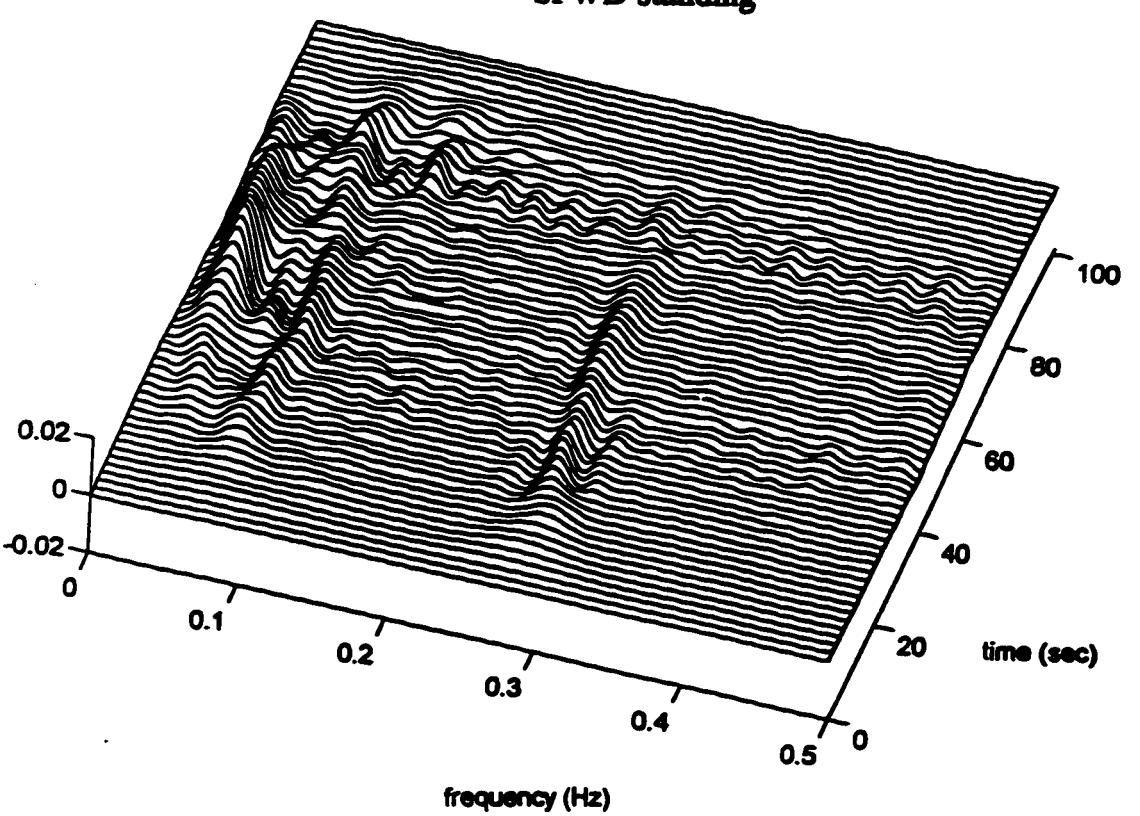

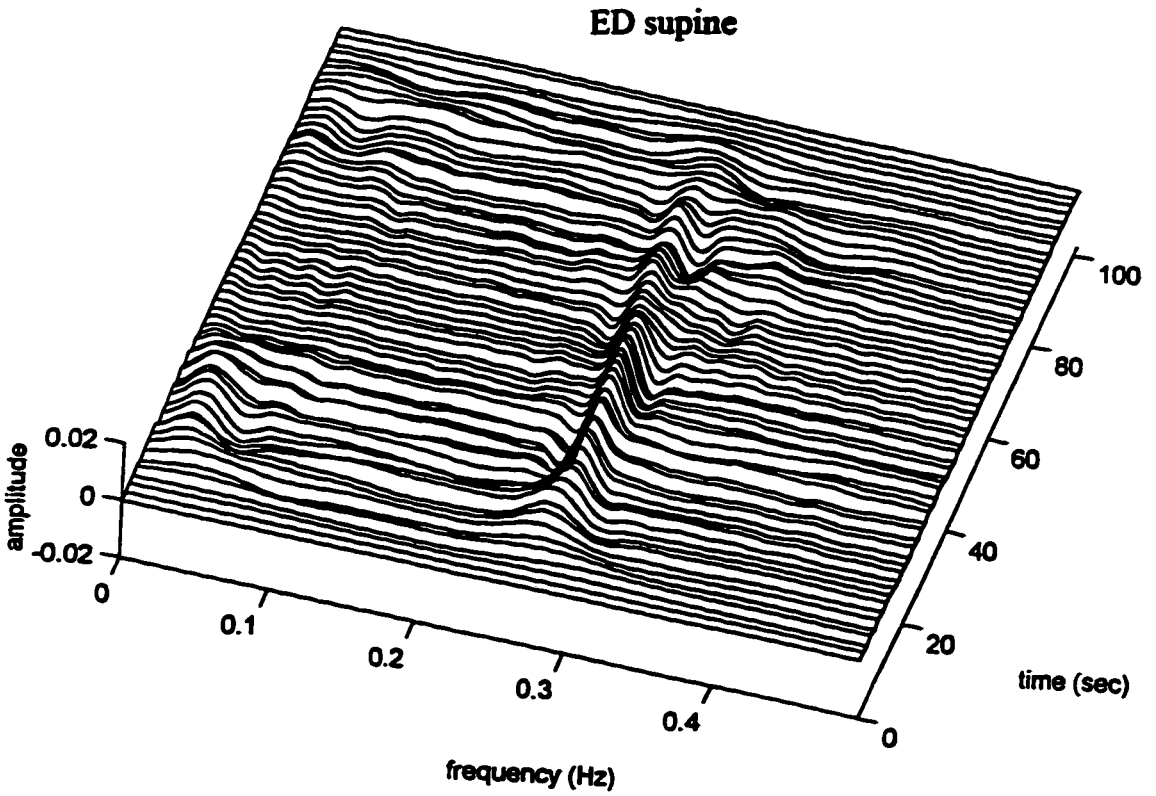
ED supine
amplitude
0.02
0
-0.02
0
0.1
0.2
0.3
0.4
frequency (Hz)
0
20
40
60
80
100
time (sec)

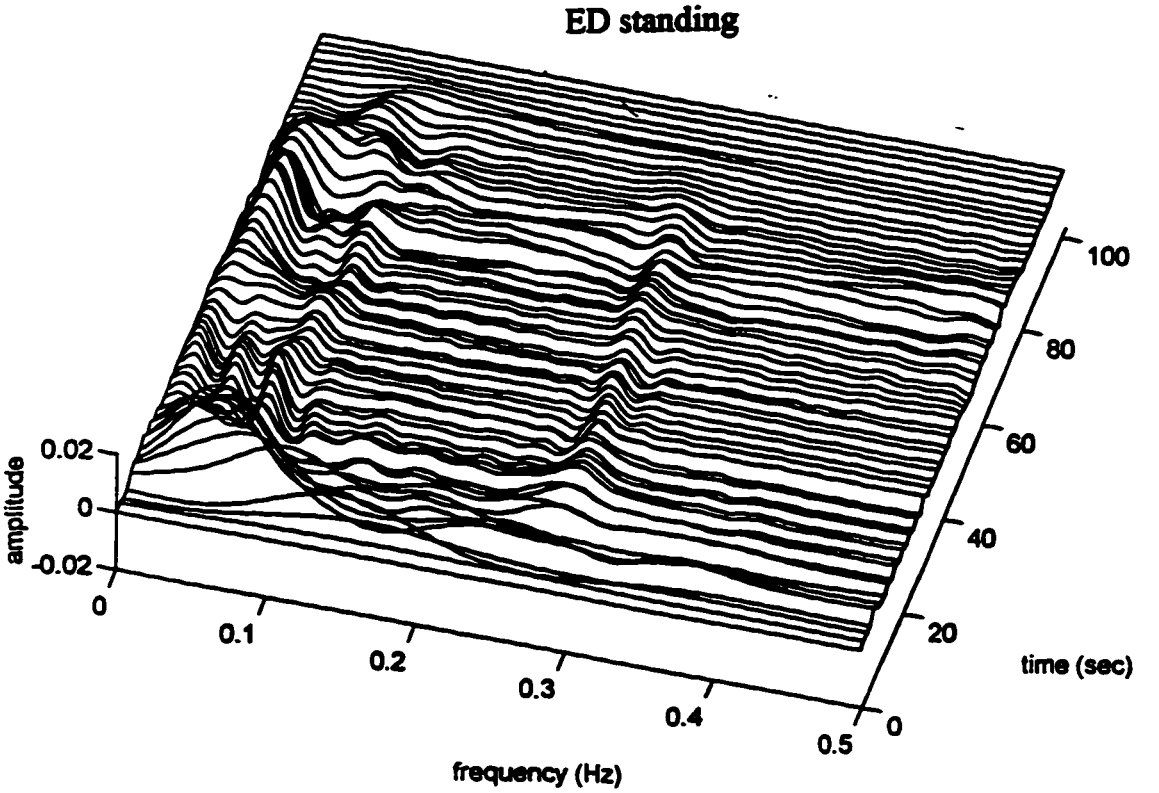
ED standing
amplitude
0.02
0
-0.02
0
0.1
0.2
0.3
0.4
0.5
frequency (Hz)
0
20
40
60
80
100
time (sec)

SPWD supine

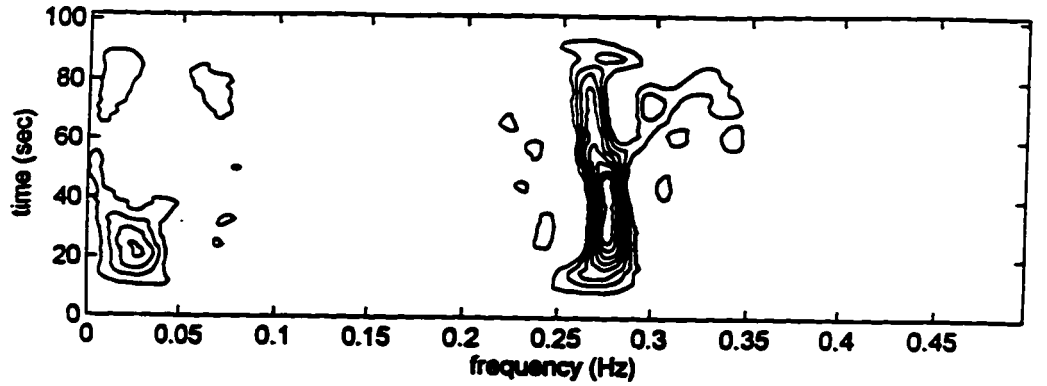

SPWD standing

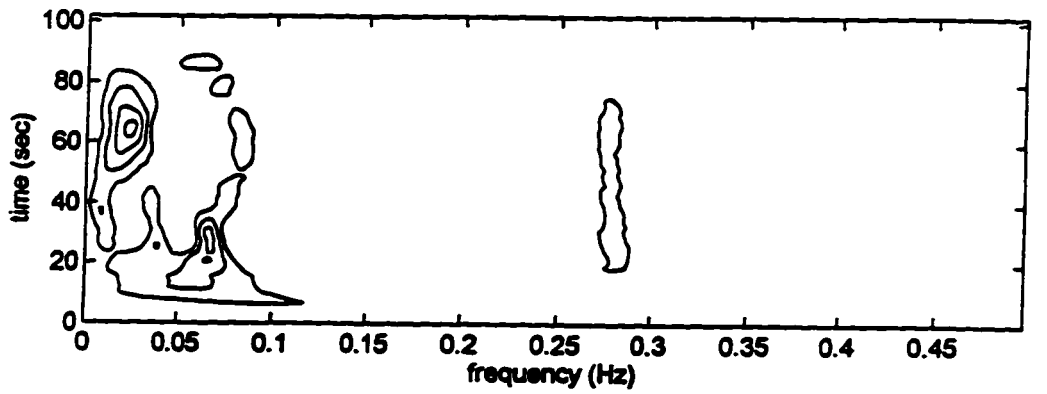

ED supine

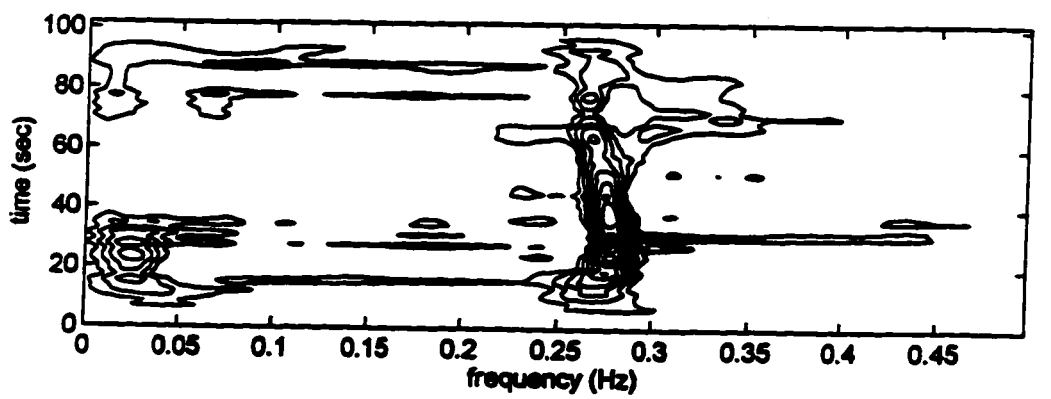

ED standing

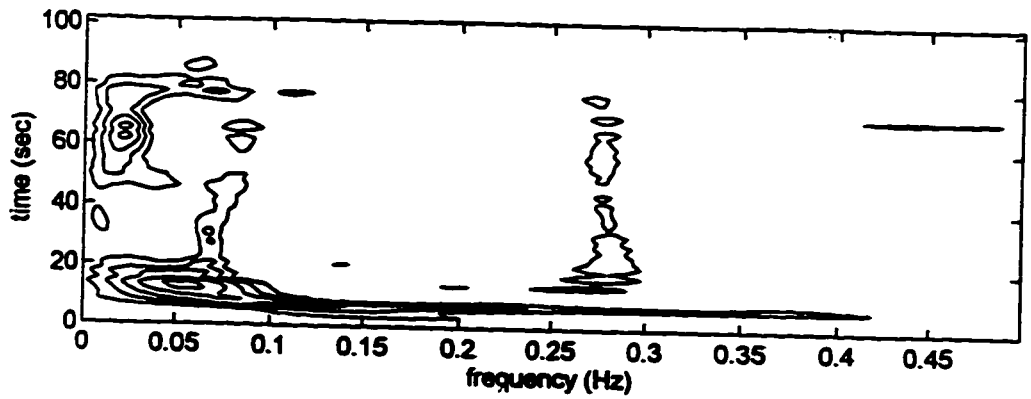

Figure 5.3 Waterfall and contour plots: Effect of posture on the HRV spectrum (SPWD and ED) under supine (increased HF component) and orthostatic stress conditions (increased LF component) with the patient (bt) HRV signal

Figure 5.4 demonstrates the effect of the stellate blockade for a patient (mg) when using the SPWD. There is a decreased LF component providing evidence of the effect of the right stellate blockade. Also this spectrum suggests that innervation to the SA node is preseved by the left stellate ganglia and higher cervical ganglia efferents.

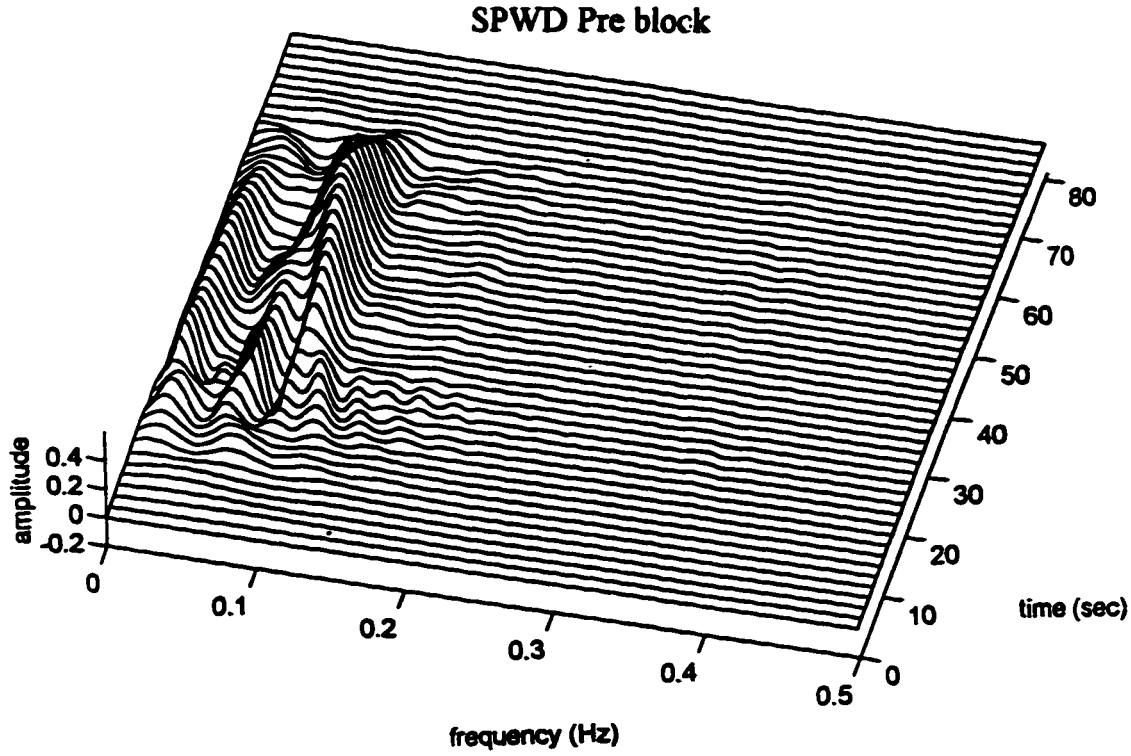
SPWD Pre block
amplitude
0.4
0.2
0
-0.2
0
0.1
0.2
0.3
0.4
0.5
frequency (Hz)
0
10
20
30
40
50
60
70
80
time (sec)

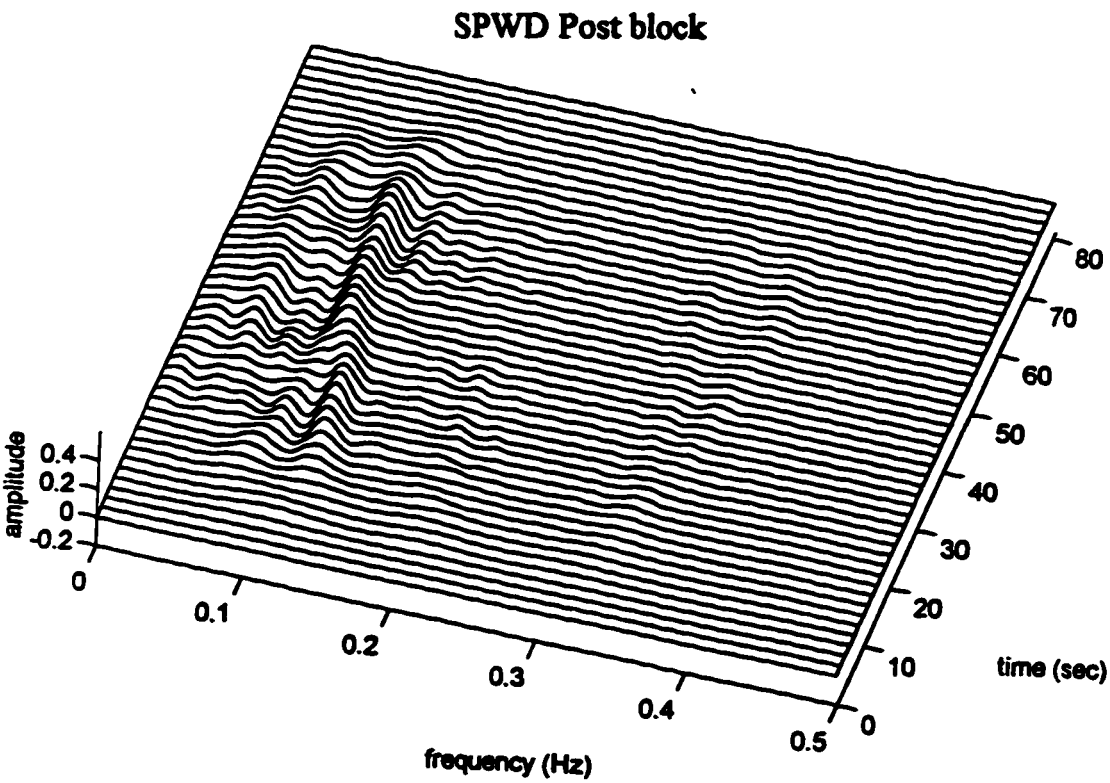
SPWD Post block
amplitude
0.4
0.2
0
-0.2
0
0.1
0.2
0.3
0.4
0.5
frequency (Hz)
0
10
20
30
40
50
60
70
80
time (sec)

SPWD Pre block

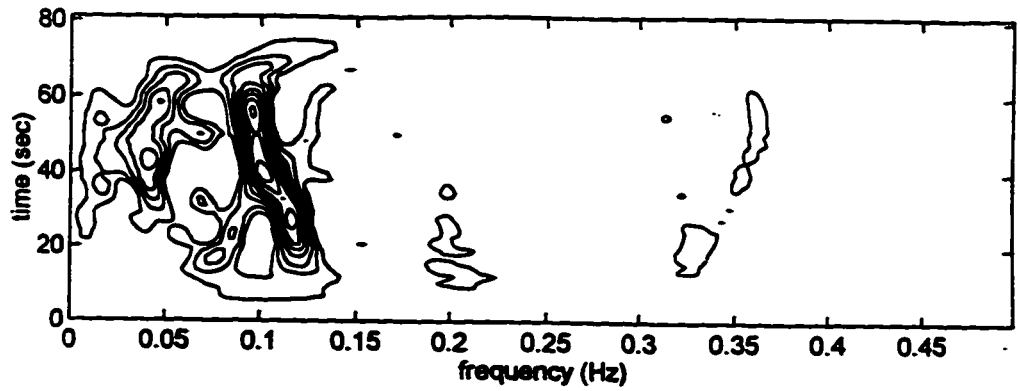

SPWD Post block

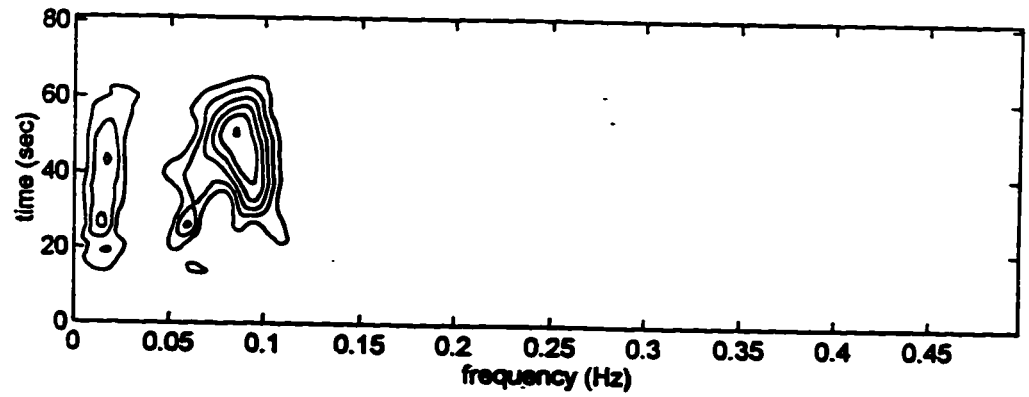

Figure 5.4 Effect of right stellate blockade for pre block and post block on a patient (mg) using the SPWD

Estimates from both these SPWD and ED methods gave comparable results for the mean peak amplitudes in each frequency band as shown in Tables 5.1,5.2, 5.3 and 5.4. When comparing the mean amplitude of the LF band from pre to post

blockade, a 33% decrease (not statistically significant) was noted between the groups under the orthostatic condition for the SPWD.

Table 5.1. Mean amplitudes in the LF,HF bands and LF/HF ratio for pre and post block subjects in the supine position using the SPWD

Patient	Pre block			Post Block		
	LF	HF	LF/HF	LF	HF	LF/HF
bt	0.0074	0.0091	0.8131	0.0051	0.0286	0.1783
dn	0.0122	0.0032	3.8125	0.0225	0.0108	2.0833
hy	0.0135	0.019	0.7105	0.0164	0.0189	0.8677
mg	0.0228	0.0937	0.2433	0.0300	0.1414	0.2121
mt	0.0064	0.0175	0.3657	0.0320	0.0111	2.8828
mw	0.0723	0.0112	6.4553	0.0712	0.0125	5.6960
wl	0.0251	0.0029	8.6551	0.0099	0.0017	5.8235
Mean	0.0228	0.0223	3.0079	0.0267	0.0321	2.5348

Table 5.2 Mean amplitudes in the LF,HF bands and LF/HF ratio for pre and post block subjects in the standing position using the SPWD

Patient	Pre Block			Post Block		
	LF	HF	LF/HF	LF	HF	LF/HF
bt	0.0314	0.0082	3.8292	0.0077	0.0056	1.3750
dn	0.0093	0.0017	5.4705	0.0402	0.0040	10.050
hy	0.0323	0.0081	3.9876	0.0464	0.0145	3.2000
mg	0.3311	0.0223	14.8475	0.1145	0.0256	4.4726
mt	0.0146	0.0164	0.8902	0.0468	0.0366	1.2786
mw	0.0356	0.0068	5.2352	0.0537	0.0145	3.7034
wl	0.0273	0.0019	14.3684	0.0127	0.0019	6.6842
Mean	0.0688	0.0093	6.9470	0.0460	0.0146	4.3948

Table 5.3 Mean amplitudes in the LF,HF bands and LF/HF ratio for pre and post block subjects in the supine position using the ED

Patient	Pre block			Post Block		
	LF	HF	LF/HF	LF	HF	LF/HF
bt	0.0089	0.0098	0.9081	0.0037	0.0192	0.1927
dn	0.0088	0.0026	3.3846	0.0187	0.0081	2.3086
hy	0.0077	0.0101	0.7623	0.0112	0.0128	0.8750
mg	0.0180	0.0654	0.2752	0.0253	0.0977	0.2589
mt	0.0049	0.0122	0.4016	0.0222	0.0079	2.8101
mw	0.0483	0.0085	5.6823	0.0566	0.0107	5.2897
wl	0.0167	0.0027	6.1851	0.0072	0.0012	6.0000
Mean	0.0161	0.0159	2.5142	0.0207	0.0225	2.5335

Table 5.4 Mean amplitudes in the LF,HF bands and LF/HF ratio for pre and post block subjects in the standing position using the ED

Patient	Pre Block			Post Block		
	LF	HF	LF/HF	LF	HF	LF/HF
bt	0.0200	0.0064	3.1260	0.0047	0.0039	1.2051
dn	0.0062	0.0013	4.7692	0.0311	0.0040	7.7750
hy	0.0253	0.0063	4.0158	0.0320	0.0097	3.2989
mg	0.2517	0.0197	12.776	0.0710	0.0206	3.4466
mt	0.0073	0.0113	0.646	0.0336	0.0255	1.3176
mw	0.0244	0.0053	4.6037	0.0392	0.0107	3.6635
wl	0.0190	0.0016	11.875	0.0085	0.0015	5.6666
Mean	0.0505	0.0074	5.9730	0.0314	0.0108	3.7676

The LH/HF ratios shown in Figures 5.5 and 5.6 demonstrates a trend of decreasing values with blockade in the standing position. In comparing these ratios between the pre block and post block group for the ED and SPWD methods, statistical significance was not reached.

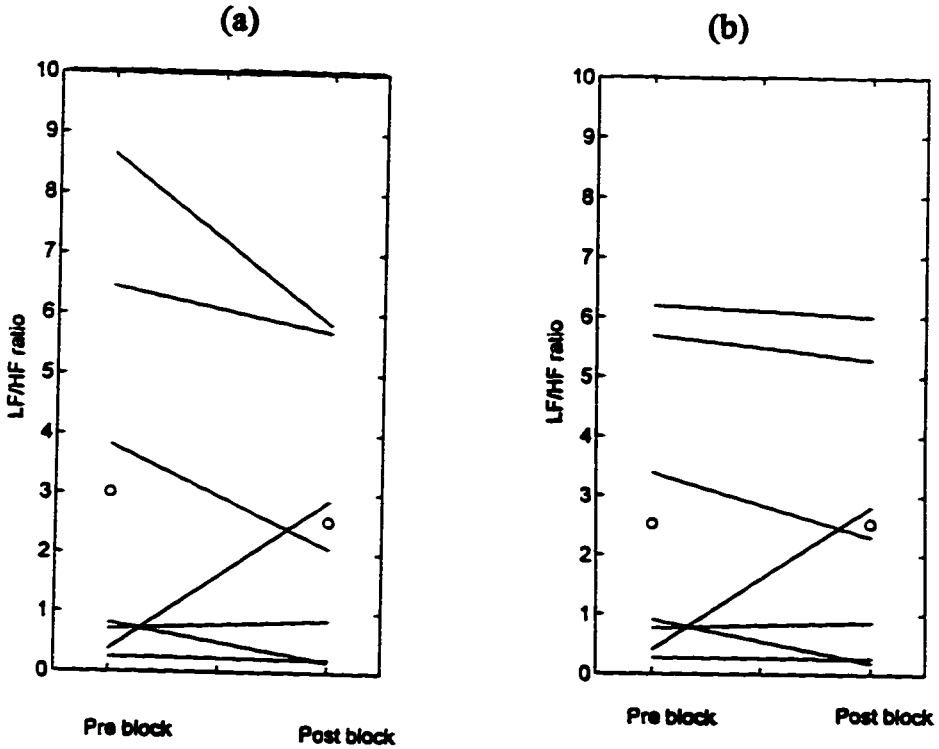

Figure 5.5 LH/HF ratio comparison for the supine position using a) SPWD and b) ED

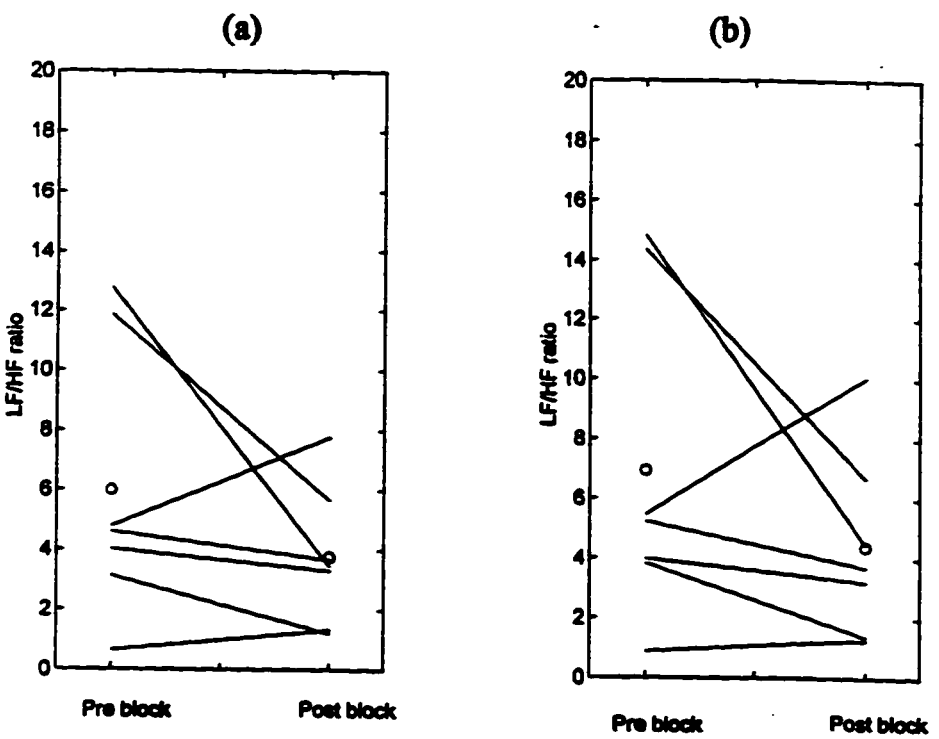

Figure 5.6 LH/HF ratio comparison for the standing position using a) SPWD and b) ED

5.4 Summary

Results suggest that although sympathetic blockade produced a slight reduction of LF power, the effects were not pronounced, even in the standing position where considerable sympathetic activity is elicited by the baroreceptor response. Pomeranz et al [Pom85] noted a 79% decrease in the area of this LF band by the use of systemic blocking drugs whereas we report a 33% decrease with stellate blockade. Therefore it maybe suggested that minimal effects on HR control are produced by unilateral stellate blockade. Sympathetic efferent originating in higher ganglia or crossing from the contralateral sympathetic chain may preserve most of the sympathetic control of HR after stellate blockade. This work has provided evidence that there is evidence of compensatory mechanisms of sympathetic tone under the effect of right stellate blockade. This preliminary study, although limited by the small study group suggests that further investigation of the stellate blockade may be warranted.

Chapter 6

6. Conclusions and Future Work

6.1 Conclusions

This thesis has introduced and investigated the application of Cohen Class TF spectral analysis distributions in the analysis of HRV signals. Simulated nonstationary and stationary HRV signals have been used to study the SPWD and ED in detail so that guidelines on the choice of the various parameters could be determined. Comparisons have demonstrated the improved performance of these methods over the popular STFT or spectrogram in terms of resolution and ability to track the IF. By definition, the WD is able to exactly track the IF. In the STFT, an approximation to the IF is obtained as a suitable data window cannot be chosen to obtain this conditional average. The tradeoff in the use of the WD is that it is plagued by cross terms or artifacts that obscure the interpretation of the spectrum. Therefore some degree of time smoothing is required at the expense of resolution. In the case of the SPWD, the use of a time smoothing window of approximately $M \approx N/2$ was sufficient to remove the artifacts The ED, a reduced interference distribution was also investigated as a potential distribution in the analysis of these signals as it preserves the IF as well as effectively reducing cross terms. It has been shown that adequate cross term suppression is achieved with $1 < \sigma < 5$. It

was also noted that these distributions are not always positive unlike the spectrogram. Therefore, in applications requiring integration to determine area under the distribution caution must be exercised.

Finally, these TF distributions were applied in a clinical study to examine the effects of unilateral stellate blockade. It was noted that these TF spectral analysis tools can provide an accurate and valuable representation of the autonomic tone in patients. The average LF and HF peak amplitudes as well as the LH/HF ratio were used as classification features in these patients.

6.1 Future Work

Although, the simulated nonstationary HRV signals provided evidence that these algorithms could track the IF, the actual patient HRV signals were taken under steady state conditions by an experienced cardiologist. Future studies should analyze these TF algorithms using a larger patient group under a host of nonsteady state conditions (patient movement, random respiration, various pathological conditions, postural studies, exercise, pharmacological studies etc.) so that the true clinical merit of the techniques can be evaluated.

One particular area where problems in the TF spectral algorithms may arise is in the analysis of transients or spikes. These were not present in the simulated or patient HRV signals. Typically, these transients introduce a broad band spectrum

and could potentially obscure the spectrum. Some researchers remove these spikes prior to spectral estimation however in certain cases these transients may carry importance clinical significance in the prognosis of the patient. For example, in the case of transient ischemic attacks these spikes carry important information which is in the form of an increased LF component just prior to the ischemic episode. It would be valuable to perform a comparative analysis of the TF algorithms to study their performance under these transient conditions.

One such TF tool that may offer promise in studying these nonstationary signals and transients are wavelets which are only recently receiving attention in the physiological signal processing field. Wavelets are unique in that they use variable length windows lengths whereby high frequency components in the signal are analyzed with sharper time resolution than low frequency components.

Chapter 7

7. References

[Abe89] Abeysekera RMSS, Boashash B: Time-Frequency Domain Analysis and Modeling of ECG Signals Using the Wigner-Ville Distribution. *ASSPA 89 Signal Processing Theories, Implementations and Applications*, 1989.

[Afo95] Afonso VX, Tompkins WJ : Detecting Ventricular Fibrillation. *IEEE Engineering in Medicine and Biology*, Mar/April, pp 152-159, 1995.

[Aks81] Akselrod S, Gordon D, Ubel FA, Shannon DC, Berger AC, Cohen RJ : Power Spectrum Analysis of Heart Rate Fluctuation: A Quantitative Probe of Beat-to-Beat Cardiovascular Control. *Science*, vol 213, pp 220-222, 1981.

[Aks85] Akselrod S, Gordon D, Madwed JB, Snidman NC, Shannon DC, Cohen RJ : Hemodynamic Regulation: Investigation by Spectral Analysis. *Am. J. Physiol.*, pp 249, H867,1985.

[Ang64] Angelone A, Coulter NA : Respiratory Sinus Arrhythmia: A Frequency Dependent Phenomenon. *J. Appl. Physiology*, vol 19, pp 479-482, 1964

[Bia90] Bianchi A ,Bontempi B, Cerutti S, Gianoglio P, Comi G, Natali Sora MG : Spectral Analysis of Heart Rate Variability Signal and Respiration in Diabetic Subjects, *Med & Biol Eng Comput.*, vol 28, pp 205-211,1990.

[Bia93] Bianchi A ,Mainardi L, Petrucci E, Signorini M, Mainardi M, Cerutti S. : Time-Variant Power Spectrum Analysis for the Detection of Transient Episodes in HRV Signal. *IEEE Transactions on Biomedical Engineering*, vol 40, no 2, pp 136, 1993.

[Big88] Bigger JT, Kleiger RE, Fleiss JL, Rolnitzky LM, Steinman RC, Miller JP : The Multicenter Post-Infarction Research Group. Components of Heart Rate Variability Measured During Healing of Acute Myocardial Infarction. *Am. J. Cardiol.*, vol 61, pp 208-215, 1988.

[Big93a] Bigger JT, Fleiss JL, Rolnitzky LM, Steinman RC : Frequency Domain Measures of Heart Period Variability to Assess Risk Late After Myocardial Infarction. *Am. J. Cardiol.*, vol 21, pp 729-36, 1993.

[Big93b] Bigger JT, Kleiger RE, Fleiss JL, Rolnitzky LM, Steinman RC. The Ability of Several Short Term Measures of RR Variability to Predict Mortality After Myocardial Infarction. *Circulation*, vol 88, pp 927-934, 1993

[Boa87] Boashash B, Black PJ : An Efficient Real-Time Implementation of the Wigner-Ville Distribution. *IEEE Transactions on Acoustics, Speech and Signal Processing*, vol. 35, no 11, 1987.

[Boa90] Boashash B : Time-Frequency Signal Analysis in: Advances in Spectrum Analysis and Array Processing, S. Haykin, Editor, Prentice Hall, 1990.

[Cho89] Choi HI, Williams WJ: Improved Time Frequency Representation of Multicomponent Signals Using Exponential Kernels. *IEEE Transactions on ASSP*, 37, pp 862-867, 1989.

[Clas80a] Classen TACM, Mecklenbrauker WFG : The Wigner Distribution- A Tool for Time-Frequency Signal Analysis Part 1: Continuos Time Signals. *Philips J. Res*, pp 217-250, 1980.

[Cla80b] Classen TACM, Mecklenbrauker WFG : The Wigner Distribution- A Tool for Time-Frequency Signal Analysis Part II: Discrete Time Signals. *Philips J. Res*, pp 276-300, 1980.

[Cla80c] Classen TACM, Mecklenbrauker WFG : The Wigner Distribution- A Tool for Time-Frequency Signal Analysis Part III. Relations with other Time-Frequency Signal Transformations. *Philips J. Res*, pp 276-300, 1980.

[Coh85] Cohen L, Posch TE : Generalized Ambiguity Functions. *Proc IEEE, Int Conf ASSP*, vol 3, 1985.

[Coh89] Cohen L : Time-Frequency Distributions - A Review. *Proceedings of the IEEE*, vol 77, no 7, pp 941-981, 1989.

[Cra92] Craelius W, Akay M, Tangella M : Heart Rate Variability as an Index of Autonomic Imbalance in Patients with Recent Myocardial Infarction. *Med & Biol Eng & Comput*, vol 30, pp 385-388,1992.

[deB85] de Boer RW, Karemaker JM, Strackee J : Spectrum of a series of point events generated by the integral pulse frequency modulation model. *Med. & Biol. Eng. & Comput.*, vol 23, pp 138-142,1985.

[Dur90] Durand LG, Langlois YE, Lanthier T, Chiarella R. Coppen P : Spectral Analysis and Acoustic Transmission of Mitral and Aortic Valve Closure Sounds in Dogs. Parts 1-4. *Med & Biol Eng & Computing*, vol 30, pp 503-508,1992.

[Fal88] Fallen EL, Kamath MV, Ghista DN, Fitchett D : Spectral Analysis of Heart Rate Variability following Human Heart Transplantation: Evidence for Functional Reinnervation. *Journal of the Autonomic Nervous System*, vol 23, pp 199-206, 1988.

[Fin87] Finley JP, Nugent ST, Hellenbrand W : Heart Rate Variability in Children. Spectral Analysis of Developmental changes between 5 and 24 years. *Can J Physiol. Pharmacol.*, vol 65, pp 2048-2052, 1987.

[Fin89] Finley JP, Nugent ST, Hellenbrand W, Craig M, Gillis DA : Sinus Arrhythmia in Children with Atrial Septal Defect: An Analysis of Heart Rate Variability Before and After Surgical Repair. *Br. Heart J.*, vol 61, pp 280-284,1989.

[Gid85] Giddens DP, Kitney RI : Neonatal Heart Rate Variability and its Relation to Respiration, *J. Theor. Biol.*, vol 113, pp 759-780, 1985.

[Har78] Harris FJ: On the Use of Windows for Harmonic Analysis with the Discrete Fourier Transform. *Proceedings of the IEEE*, vol 66, no 1, 1978.

[Hla92] Hlawatsch F, Boudreaux-Bartels GF: Linear and Quadratic Time-Frequency Signal Representations. *IEEE SP Magazine*, April, pp 21-67, 1992.

[Hui93] Huikuri HV, Valkama JO, Airaksinen J, Seppanen T, Kessler KM, Takkunen JT, Myerburg RJ: Frequency Domain Measures of Heart Rate Variability Before the Onset of Nonsustained and Sustained Ventricular Tachycardia in Patients With Coronary Artery Disease. *Circulation*, vol 87, no 4, pp 1220-1228, 1993.

[Jan86] Janes RD, Brandys JC, Hopkins DA, Johnstone DE, Murphy DA, Armour JA : Anatomy of Human Extrinsic Cardiac Nerves and Ganglia. *Am J Cardiolology*, vol 57, pp 299-309, 1986.

[Jeo92] Jeong J, William WJ : Kernel Design for Reduced Interference Distributions. *IEEE Transactions on Signal Processing*, vol 40, no 2, pp 402-412, 1992.

[Joh87] Johnstone DE, Montague TJ, Shukla RC, Gardner MJ, Janes RD, Armour JA : Cardiac Effects of Stellate Ganglia Imbalance. *Clin Invest Med*, vol 10, C68, 1987.

[Jon92] Jones DL, Parks TW : A Resolution Comparison of Several Time-Frequency Representations. *IEEE Transactions on Signal Processing* vol 40, no 2, pp 413-420, 1992.

[Kay81] Kay SM, Marple SL Spectrum Analysis- A Modern Perspective. Proceedings of the IEEE, vol. 69, no. 11, pp 1380-1419. 1981.

[Kit85] Kitney RI, Fulton T, MacDonald AH, Linkens DA : Transient Interactions between Blood Pressure, Respiration and Heart Rate in Man, *Journal of Biomedical Engineering*, vol 7, pp 217,1985.

[Kit92] Kitney RI, Bignall S. Techniques for Studying Short-Term Changes in Cardiorespiratory Data. Blood Pressure and Heart Rate Variability. ed. M Di Rienzo. IOS Press, 1992.

[Kle87] Kleiger RE, Miller JP, Bigger JT, Moss AJ and the Multicenter Research Group : Decreased Heart Rate Variability and its Association with Increased Mortality After Acute Myocardial Infarction, *Am J Cardiol*; vol 59, pp 256-262, 1987.

[Lom87] Lombardi, F, Sandrone G, Pernpruner S, Sala R, Garimoldi M, Cerutti S, Baselli G, Pagani M, Malliani A: Heart Rate Variability as an Index of Sympathovagal Interaction After Acute Myocardial Infarction. *Am. J. Cardiol.*, 60, pp 1239-1245, 1987.

[Mal90] Malik M, Farrell T, Camm AJ : Circadian Rhythm of Heart Rate Variability After Acute Myocardial Infarction and Its Influence on the Prognostic Value of Heart Rate Variability. *Am. J. Cardiol.*, vol. 66, pp 1049-1054, 1990.

[Mar91] Marchesi C, Venturi M, Pola S, Conforti F, Macerata A, Varanini M, Emdin M : Sequential Estimation of the Power Spectrum for the Analysis of Variability of Nonstationary Cardiovascular Signals. *Annual International Conference of the IEEE Engineering in Medicine and Biology Society*, vol 13, no 2, 1991

[Mye86] Myers GA, Martin GJ, Magid NM, Barnett PS, Schaad JW, Weiss JS, Lesch M, Singer DH : Power Spectral Analysis of Heart Rate Variability in

Sudden Cardiac Death: Comparison to Other Methods, *IEEE Transactions on Biomedical Engineering*, vol.33, no 12, pp 1149-1156, 1986.

[Nov93] Novak P, Novak V. Time/Frequency Mapping of the Heart Rate, Blood Pressure and Respiratory Signals. *Medical & Biological Engineering and Computing*, vol 31, March, pp 103-110, 1993

[Nug86] Nugent ST, Finley JP: Position Induced Changes in the Heart Rate Spectrum of Young Children. 12th C.M.B.E.C./ 1st Pan. Pacific Symposium. Vancouver, Canada, pp 126-127, 1986.

[Pom85] Pomeranz B, Macaulay RJ, Caudill M, Kutz I, Adam D, Gordon D, Kilborn KM, Barger AC, Shannon DC, Cohen RJ, Benson H : Assessment of Autonomic Function in Humans by Heart Rate Spectral Analysis. *Am J. Physiology*, vol 248, H151-H153, 1985.

[Rom77] Rompleman O, Coenen AJRM, Kitney RI: Measurement of Heart Rate Variability: Part 1-Comparative Study of Heart-Rate Variability Analysis Methods. *Med. & Biol. Eng. & Comput.*, 15, pp 233-239,1977.

[Rom87] Rompleman O : Accuracy Aspects in ECG Pre-processing. The Beat-by-beat Investigation of Cardiovascular Function. Eds Kitney RI and Rompleman O, Oxford University Press, Oxford, pp 103-125, 1987.

[San86] Sands KEF, Lily LS, Schoen FJ, Mudge GH, Cohen RJ : Heart Rate Variability in Stable and Rejecting Cardiac Transplant Recipients. *JACC*, 7,190A, 1986.

[Sau88] Saul JP, Arai Y, Berger RD, Lilly LS, Colucci WS, Cohen RJ.Assessment of Autonomic Regulation in Chronic Congestive Heart Failure by Heart Rate Spectral Analysis. *Am J. of Cardiology*, vol 61,pp 1292-1299,1988.

[Sau89] Saul JP, Berger RD, Chen MH, Cohen RJ : Transfer Function Analysis of Autonomic Regulation II. Respiratory Sinus Arrhythmia. *Am J of Physiology*, vol 256, H153-H161, 1989.

[Sch87] Schwartz PJ. Manipulation of the Autonomic Nervous System in the Prevention of Sudden Cardiac Disease. In Cardiac Arrhythmias: Where to go from here? Brugada P, Wellens HJJ. eds Futura Publishing Co. Mount Kisco NY pp 741-764, 1987.

[Sin88] Singer DH, Martin GJ, Magid N, Weiss JS,Schaad JW, Kehoe R, Zheutlin T,Fintel DJ, Hsieh A, Lesch M : Low Heart Rate Variability and Sudden Cardiac Death, *Journal of Electrocardiology*, S46-S55, 1988.

[Sta93] Stankovic L, Stankovic S: Wigner Distribution of Noisy Signals. *IEEE Transactions on Signal Processing*. vol 41, no 2, pp 956-960, 1993.

[Van83] Van den Akker TJ, Koeleman AJM, Hogenuis LAH, Rompleman O. Heart Rate Variability and Blood Pressure Oscillation in Diabetics with Autonomic Neuropathy. *Automedica*, vol 4, pp 201-208,1983.

[Van87] Van der Schee EJ. Running Spectrum Analysis as an Aid in the Representation and Interpretation of Electrogastric Signals. *Med & Biol Eng Comp*, vol 25, pp 57-62, 1987.

[Ven91] Venturi M, Conforti F, Macerata A, Varanini M, Emdin M, Marchesi C : Analysis of Variability: A System for comparing Classical, Parametric, Adaptive and Wigner-Ville Power Spectral Estimators,Computers in Cardiology. *IEEE Computer Society*, pp 247-250, 1991.

[Vyb89] Vybiral T, Bryg RJ, Maddens ME, Boden WE : Effect of Passive Tilt on Sympathetic and Parasympathetic Components of Heart Rate Variability in Normal Subjects. *Am J of Cardiology*, vol 63, pp 1117-1120, 1989.

[Wan95] Wang X, Sun HH, Van de Water JM : Time-Frequency Distribution Technique in Biological Signal Processing. *Biomedical Instrumentation and Technology*, vol 29, no 3, pp 203-212, 1995.

[Wil95] Williams WJ, Zaveri HP, Sackellares JC : Time-Frequency Analysis of Electrophysiology Signals in Epilepsy. *IEEE Engineering in Medicine and Biology*, March/April, pp 133-143, 1995.